1.0

1.1

1.25

4.5
5.0
5.6

2.8
3.2
3.6
4.0

2.5
2.2
2.0
1.8

1.4

1.6
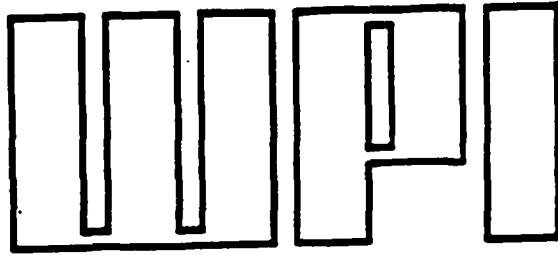
MICROCOPY   CHART

WORCESTER
POLYTECHNIC
INSTITUTE

CHARACTERIZATION OF ION IMPLANTED AND
LASER PROCESSED WEAR SURFACES

Final Report: Contract No. N00014-85-K-0066

Submitted to:

Office of Naval Research
Materials Division, Code 431M
800 N. Quincy Street
Arlington, VA 22217

Submitted by:

Sara A. Dillich

Department of Mechanical Engineering
Worcester Polytechnic Institute
Worcester, Massachusetts 01609

April, 1986

DTIC
SELECTE
MAY 2 0 1986
E

WORCESTER POLYTECHNIC INSTITUTE • WORCESTER, MASSACHUSETTS 01609 •

CHARACTERIZATION OF ION IMPLANTED AND LASER
PROCESSED WEAR SURFACES

Final Report: Contract No. N00014-85-K-0066

Submitted to:

Office of Naval Research
Materials Division, Code 431M
800 N. Quincy Street
Arlington, Va. 22217

Submitted by:

Sara A. Dillich

Department of Mechanical Engineering
Worcester Polytechnic Institute
Worcester, Mass. 01609

Accession For	
NTIS GRA&I	X
DTIC TAB	☐
Unannounced	☐
Justification	

By	
Distribution/	
Availability Codes	
	Avail and/or
Dist	Special
A-1	

April, 1986

QUALITY INSPECTED 3

REPORT DOCUMENTATION PAGE		READ INSTRUCTIONS BEFORE COMPLETING FORM
1. REPORT NUMBER	2. GOVT ACCESSION NO. ADA 167898	3. RECIPIENT'S CATALOG NUMBER
4. TITLE (and Subtitle) CHARACTERIZATION OF ION IMPLANTED AND LASER PROCESSED WEAR SURFACES		5. TYPE OF REPORT & PERIOD COVERED Final Report 12/01/84 - 2/28/86
		6. PERFORMING ORG. REPORT NUMBER
7. AUTHOR(s) Sara A. Dillich		8. CONTRACT OR GRANT NUMBER(s) N00014-85-K-0066
9. PERFORMING ORGANIZATION NAME AND ADDRESS Department of Mechanical Engineering Worcester Polytechnic Institute Worcester, Mass 01609		10. PROGRAM ELEMENT, PROJECT, TASK AREA & WORK UNIT NUMBERS 091-053
11. CONTROLLING OFFICE NAME AND ADDRESS Office of Naval Research, Code 431M 800 N. Quincy Street Arlington, Va. 22217		12. REPORT DATE 4/22/86
		13. NUMBER OF PAGES 40
14. MONITORING AGENCY NAME & ADDRESS(If different from Controlling Office)		15. SECURITY CLASS. (of this report) unclassified
		15a. DECLASSIFICATION/DOWNGRADING SCHEDULE

16. DISTRIBUTION STATEMENT (of this Report)

unlimited

17. DISTRIBUTION STATEMENT (of the abstract entered in Block 20, if different from Report)

18. SUPPLEMENTARY NOTES

19. KEY WORDS (Continue on reverse side if necessary and identify by block number)

ion implantation, laser processed surfaces, wear, tribology, cavitation erosion, amorphization, carbides

20. ABSTRACT (Continue on reverse side if necessary and identify by block number)

SEM/EDX and scanning Auger microscope analysis were employed to characterize wear surfaces and debris on friction tested, laser processed metal-carbide composite surfaces. The friction and wear of the composite samples were found to be influenced by the compatibility (degree of mutual solubility) of the carbides with the steel counterface, as well as by local inhomogeneities in the carbide distribution. High fluence Ti implantation resulted in increased friction and wear, possibly due to an

DD FORM 1473 EDITION OF 1 NOV 65 IS OBSOLETE
S/N 0102-LF-014-6601

implantation induced softening or degradation of the carbides.

Cavitation erosion tests were performed on nonimplanted and ion implanted samples of a Co-based hardface alloy (Stoody 3). Erosion of the test samples was found to initiate by debonding at the carbide-matrix interfaces and by crack propagation through the carbides. The erosion mechanisms in the alloy were altered by both N and Ti implantations. Ti implantation, in particular, appeared to significantly increase the erosion resistance of the alloy.

TEM studies were made on nonimplanted and ion implanted foils of Stoody 3, to investigate structural changes induced by implantation. Ti implantation produced a surface layer with an amorphous matrix phase and recrystallized carbides, while N implantation greatly increased the stacking fault density in the matrix phase.

TABLE OF CONTENTS

ABSTRACT

        SEM/EDX and scanning Auger microscope analysis were employed to
characterize wear surfaces and debris on friction tested, laser processed
metal-carbide composite surfaces. The friction and wear of the composite
samples were found to be influenced by the compatibility (degree of mutual
solubility) of the carbides with the steel counterface, as well as by local
inhomogeneities in the carbide distribution. High fluence Ti implantation
resulted in increased friction and wear, possibly due to an implantation
induced softening or degradation of the carbides.
        Cavitation erosion tests were performed on nonimplanted and ion
implanted samples of a Co-based hardface alloy (Stoody 3). Erosion of the
test samples was found to initiate by debonding at the carbide-matrix
interfaces and by crack propagation through the carbides. The erosion
mechanisms in the alloy were altered by both N and Ti implantations. Ti
implantation, in particular, appeared to significantly increase the erosion
resistance of the alloy.
        TEM studies were made on nonimplanted and ion implanted foils of
Stoody 3, to investigate structural changes induced by implantation. Ti
implantation produced a surface layer with an amorphous matrix phase and
recrystallized carbides, while N implantation greatly increased the stack-
ing fault density in the matrix phase.

ii

ACKNOWLEDGEMENTS

LIST OF FIGURES

v

INTRODUCTION

The goals of this work were twofold: to investigate the tribological characteristics of metal/carbide materials and to determine how they may be altered by high fluence ion implantation. To this end, two metal/carbide systems were studied; model transition metal/carbide composites prepared by the Laser Melt Particle Injection (LMPI) process, and a Co-based (Co-31Cr-12.5W-2.2C) alloy, Stoody 3. Implantations for this study, were made with titanium or nitrogen, ionic species which have been found to improve the tribology of steels (1-3). All implantations were performed at the Naval Research Laboratory in Washington, D.C.

Dry sliding friction tests were performed on LMPI samples containing 24 to 42 volume % carbide. The specific contributions of the carbide and metal phases to the friction and wear of the LMPI samples were investigated via SEM/EDX and Scanning Auger Microscopy (SAM) examinations of wear surfaces and debris. Friction tests and surface analyses were again performed on the LMPI samples following Ti implantation. The results of these investigations are summarized in the next section of this report.

Co-based alloys are among the most wear resistant materials commercially available. These alloys consist of hard Cr and W carbides (primarily M_7C_3 and M_6C) dispersed in softer, more ductile, Co-rich solid solutions. Although Co-Cr-W solid solutions normally have hcp structures at low temperatures; for most applications, the alloys are designed to have the more ductile metastable fcc phase. The superior abrasion and erosion resistance of these alloys is attributed to their low stacking fault energies which allow low temperature, localized martensitic fcc-hcp transformations to occur with strain at an abraded or eroded surface (4-6). Thus, it is believed, the ductile bulk alloys are protected by surfaces with high strain hardening characteristics. The high costs of these materials, however, as well as the uncertainties in the cobalt market, are incentives for further study and, if possible, improvement of the wear resistance of these alloys.

Previous work performed at the Naval Research Laboratory employed dry sliding friction tests and abrasive wear measurements to study the effect of implantation on the Stoody 3 alloy. The abrasion resistances of nitrogen

and titanium implanted samples, relative to that of the nonimplanted alloy can be seen in Fig. 1. Ti implantation (5×10^{17} Ti/cm^2, 190 keV) of the alloy created abrasion resistant surfaces (Fig. 1a) which also exhibited a 50 - 70% reduction in dry sliding friction (7-9). Scanning Auger microscope analysis revealed that a vacuumcarburized titanium layer was produced on the alloy in both matrix and carbide phases during implantation (7). Similar vacuum-carburized (Fe-Ti-C) surfaces found on Ti implanted steels were shown to be amorphous (10-11). However, the existence of disordered phases in Ti implanted Stoody 3 surfaces, and the specific role of the carburized layers in the establishment of a low friction and wear characteristic in the alloy, remained to be determined.

In contrast, the abrasive wear resistance of the Stoody 3 alloy dropped to about 1/2 the bulk value after nitrogen implantation (4×10^{17} N/cm^2, 50 keV). Changes in the wear mode during dry sliding were also observed after implantation, although the friction remained high (9). Nitrogen stabilization of the metastable fcc matrix phase, with a resultant decrease in surface workhardening during sliding and abrasion, was offered as a possible, but unproven, explanation of the observed behavior (9). Since nitrogen has little or no solid solubility in cobalt, its effects as a phase stabilizer have not been documented. However, nitrogen stabilization of the fcc phase in the binder alloy of a N implanted Co-cemented tungsten carbide has been reported (12).

The abrasive wear tests discussed above yielded little information on the wear mechanisms active in the alloy; other than that they can be altered by ion implantation. In order to aid in the determination of characteristic wear modes in metal/carbide composite alloys, and to further study the effects of ion implantation on the tribology of the alloy, cavitation erosion tests were performed on nonimplanted and ion implanted Stoody 3 samples.

Finally, Transmission Electron Microscope (TEM) analyses of non implanted and implanted Stoody 3 foils were performed to determine implantation induced microstructural changes responsible for the observed abrasion and erosion behavior of the implanted alloy surfaces.

SUMMARY OF WORK PERFORMED

Laser Processed Surfaces

The intent of this study was to identify the contributions of carbide
and matrix phases to the galling friction and wear of carbide strengthened
alloys. Low speed, dry sliding friction measurements were made on model
carbide/metal matrix composites tested against 52100 steel, followed by
light and electron microscope examinations of the wear scars. Wear debris
on the worn surfaces were analysed using SEM/EDX and Auger Scanning
Microscopy (SAM). This work was performed in collaboration with Dr. Irwin
L. Singer of the Chemistry Division of the Naval Research Laboratory.

The composite samples were prepared at the Naval Research Laboratory
by the Laser Melt Particle Injection (LMPI) Process. The samples contained
24 to 42 volume % carbides (TiC or WC) injected into Ti or Al alloy
surfaces (13-14). The large size of the carbides (on the order of 100
microns) allowed for easy identification of the separate phases during
optical and electron microscope examinations.

As was discussed previously, ion implantation is a recently developed
surface modification technique which has been found to improve the tri-
bology of engineering alloys (1-3,9). However, the influence of implanta-
tion on the separate phases of metal/carbide alloy systems with conven-
tionally sized carbides is not easily deduced. To aid in this determina-
tion, and in the characterizaton of the tribology of the steel -
metal/carbide couples, friction tests were also made on the LMPI samples
after high fluence Ti implantation.

The details of the experimental procedure used in this work, and of
the test results can be found in Ref. 15 (see enclosed reprint). The
conclusions of the study are summarized below.

1. High galling wear resistance during dry sliding against steel is
    provided by high carbide volume % LMPI carbide/metal composites.
    However, since carbide poor regions serve as nucleation sites for
    adhesive wear inhomogeneities in carbide density are an important
    factor in the determination of their galling wear resistance.

2. The TiC /Ti surface exhibited lower friction and wear than did the WC/Ti or TiC/Al surfaces. This can be attributed to the superior hardness of this surface, and to the lower degree of compatability (i.e. mutual solid solubility) of TiC/steel couples, as compared to WC/steel couples.

3. Stickslip friction, the result of adhesive micro-welding at the contact interface, can occur when the reactivity of the materials is very great (as was the case during initial contact on the samples following implantation). Severe stickslip, leading to high frictional losses, however, is most often indicative of large amounts of debris coverage on both counterfaces with resulting debris-debris contact and concommitant increases in contact area, adhesion and backtransfer.

4. High fluence Ti-implantation produced increased friction and wear of the LMPI surfaces as a result of the a) enhanced reactivity of the surfaces provided by the excess Ti and b) softening of the carbides.

Cavitation Erosion Tests

Cavitation erosion test equipment (vibrating horn configuration) was purchased, assembled, and calibrated according to ASTM standard G32-85. Tests were performed on both implanted and nonimplanted Stoody 3 samples under standard test conditions (20 kHz frequency, 0.05 mm amplitude displacement). The test liquid, distilled water, was kept at 20 ± 2 ^{o}C by means of a cooling coil immersed in the test beaker. Test conditions deviated from the standard in one respect: due to the extreme hardness and non-machineability of the alloy, samples were not attached to the horn by means of a threaded end. Rather, test samples were held stationary below the vibrating horn. In addition to being convenient, this configuration also avoided the disadvantages of the moving sample geometry e.g., stress imposed by the longitudinal vibrations of the horn even in the absence of cavitation (16) and rimming (nonuniform erosion of the sample due to an undamaged annular region around the perimeter of the sample).

Test samples were disks 1.27 cm in diameter by 0.27 cm thick. Before testing, the sample surfaces were diamond polished to a 1 micron diamond finish and cleaned with organic solvents. Nitrogen and titanium implantations were made to fluences of 4×10^{17} N/cm^2 at 50 keV, and $5 \, 10^{17}$ Ti/cm^2 at 190 keV, respectively. The loss in mass of the samples due to cavitation was monitored during testing by periodic weighing of the samples. Erosion depths of the samples were calculated using the bulk density of the Stoody alloy (8.63 gr/cm^3) and the total area of the test surface (5.1 cm^2). Cumulative erosion depths of nonimplanted and implanted Stoody 3 samples, run to total test times between 15-25 hours, are shown in Fig. 2. Weight loss measurements after 5 hours of testing were made with a digital scale readable to $\pm$ 0.1 milligram. Thereafter, a scale accurate to $\pm$ 0.01 milligram was used. Scanning electron micrographs of the eroded surfaces can be seen in Figures 3-8.

Tests were interrupted every hour for the first 10 hours of testing for inspection and/or weighing of the samples, and every 2.5 hours thereafter. The exception was the nonimplanted sample #1 (Fig. 2) which was tested continuously for 20 hours before weighing. The difference in the

rates of weight loss of the two nonimplanted samples (#1 & #2) shown in Fig. 2 suggests that the rate of mass loss varies with the length of the exposure interval. The incubation period (test time before weight loss is observed) was 10 hours for the nonimplanted sample (#2); however, damage to the surface could be observed after the first hour of testing. SEM inspection of the eroded surface indicated that erosion initiated by crack propogation through the carbides and by debonding at the carbide-matrix interfaces (Fig. 3). After 25 hours of testing, considerable damage to the Co-rich matrix phase was also observed (Fig. 4).

Little difference in the weight loss characteristic of the alloy was detected after N implantation (Fig. 2). However, a significant change in the appearance of the eroded surface was observed during the first hours of testing. The N implanted surface suffered an "exfoliation" process by which a thin surface layer was lost from both carbide and matrix phases. The last stages of this phenomenon can be seen in Fig. 5. The debonding and carbide crack growth processes observed on the nonimplanted sample were delayed on the N implanted sample. However, these erosion mechanisms were eventually observed after about 10-15 hours of testing (Fig. 6).

Even more dramatic changes in erosion behavior were observed after Ti implantation. The cumulative depth of erosion was much lower for this sample than for the others (Fig. 2). Although crack propogation in the larger carbides was observed, debonding at the carbide-matrix interfaces was not (Fig. 7). Apparently, material loss occurred primarily at the carbide crack sites (Figs. 7&8). Only after 20 hours of testing was damage to the matrix observed, and then much less than in the nonimplanted sample (Compare Figs. 4 & 8). However, as was the case for the nonimplanted sample, surface damage progressed rapidly after the appearance of matrix phase erosion. Indeed, separate phases on the eroded surface were barely distinguishable after 35 hours of cavitation; although, surprisingly, carbide-matrix phase cohesion persisted (Fig. 9). The preliminary tests described above demonstrate that high fluence ion implantation produces significant changes in the cavitation erosion behavior of the Stoody alloy primarily, it appears, by toughening the matrix phase, and inhibiting debonding between matrix and carbide phases. A proposal has ueen submitted to the Office of Naval Research to continue the study of the effects of implantation on erosion mechanisms of n etal/carbide systems.

TEM Investigations

Microstructural changes produced by high fluence implantations of Stoody 3 were investigated by TEM examinations of nonimplanted and implanted foils of the alloy. The foils (3mm diameter, 0.1 mm thick) were punched from 12.7 mm diameter buttons, hand ground, and then polished on both sides to < 1 micron finish. Implant conditions for the foils were chosen to correspond to those used in the wear and erosion studies i.e., 5 x 10^{17} Ti/cm^2 at 190 keV or 4 x 10^{17} N/cm^2 at 50 keV. The samples were heat sunk onto a water cooled holder during implantation to limit the temperature rise at the surfaces to $\leq$ 50 °C.

The foils were thinned by one-sided electropolishing, at 50 °C, in a solution of 15% HNO_3 in Methanol. Plastic "dummy" foils protected the surface of interest (i.e., the implanted surface or, in the case of non-implanted foils, the as-polished surface) from the electrolyte during thinning. Thinned regions on the foils were examined in a 100 kV electron microscope (JEOL 100C STEM). Transmission of electrons at this energy is limited to regions of $\approx$ 150 nm maximum thickness i.e., corresponding to the range of ion penetration on the implanted surfaces (7). Microstructural features of the nonimplanted material were examined to establish a reference for the implanted surfaces. SEM micrographs of a nonimplanted foil, are shown in Fig. 10. Several distinct carbide morphologies can be distinguished in the alloy: large dark lath or block shaped carbides, a light "script" phase, and smaller light and dark elliptically shaped carbides dispersed between the larger carbides. EDX analysis revealed the metal components of the carbides to be Cr-Co-W solutions, with the lighter appearing carbides having higher W concentrations than the darker. Exact stoichiometries of these carbides have yet to be determined.

Bright field TEM micrographs and Selected Area Diffraction (SAD) patterns from nonimplanted foils are shown in Figs. (11-13). The matrix phase of the alloy is characterized by networks of planar defects, predominantly stacking faults, running through the grains, extending occasionally from one matrix grain to another (Fig. 11). Dislocation tangles could be found, infrequently, in combination with the stacking faults or concentrated at grain boundaries (Fig. 11). At present, faults and dislocations in the alloy have not been fully characterized. Single crystal diffraction

patterns from the cobalt-rich matrix phase indicated only the presence of the metastable fcc phase (e.g., Fig. 12), suggesting that cold working during the polishing process was not sufficiently severe to produce the martensitic fcc-hcp transformation at the surface. The large carbides appeared semi-opaque and virtually defect free. SAD patterns from these carbides (Fig. 13) were typical of those produced by single crystal complex carbides.

In order to investigate the effects of cold work deformation on the alloy microstructure, observations were also made on an unpolished (600 grit SiC paper finish) foil (Fig. 14). A much denser dislocation sub-structure was observed in this foil than in the fine polished samples (Compare Figs. 12 and 14). Deformation of the sample surface produced streaking and ring segments on the SAD patterns. Again, the cubic phase was predominant in all patterns from the matrix phase (Fig. 14), however the presence of extra spots and streaks superimposed on the basic fcc pattern suggests the possibility that the fcc matrix contained some regions of transformed hcp material.

The effects of Ti implantation on the alloy microstructure are shown in Figs. 15-18. Implantation produced an amorphous matrix phase, as evidenced by the diffuse rings in the SAD patterns from this phase, and by the absence of defects i.e., dislocations and planer faults (Fig. 15). Similarly, the carbides were transformed from monolithic single crystals to fine-grained polycrystals (Figs. 16 & 17), with diffraction spots forming ring patterns (Fig. 17). Partial amorphization of the carbide surfaces is suggested by the diffuse nature of the rings. The carbides were outlined by borders of light contrast, matrix material which, on close inspection, appeared carbide depleted. EDX analysis of the border region shown in Fig. 18 indicated higher Ti concentrations in the carbides and bordering matrix than for the neighboring, darker contrast matrix material. Preferential carburization (i.e., the formation of a Ti + C enriched surface layer (7)) at or near the carbides during implantation is a possible explanation of this result.

Micrographs from a N implanted foil can be seen in Figs. 19 & 20. Single crystal SAD patterns were obtained from both matrix and carbide phases on the foil. As was the case for the nonimplanted foils, the matrix phase was found to be cubic (Fig. 19). Although N implantation did not

produce changes in the crystallinity of the surface, a striking increase in the fault density was observed (Compare Figs. 19 & 20 with Figs. 11 & 12).

The TEM investigations described above revealed significant microstructural changes in the alloy after both N and Ti implantations. Additional examination of implanted foils is, of course, needed to test the consistency of the results. Nevertheless, some discussion and concluding remarks concerning the effects of implantation microstructures on the properties of the alloy is presented below.

Ti implantation modified the chemistry of the Stoody 3 surface via carburization i.e., the introduction of excess carbon atoms into the surface during implantation (7). Microstructural changes were also produced, most notably a noncrystalline matrix phase the result, presumeably, of ion bombardment damage to the original crystalline lattice. This amorphous carburized layer provided a low friction, wear resistant alloy surface, as shown by dry sliding friction, abrasion and cavitation erosion tests.

Examination of cavitation eroded Stoody 3 surfaces showed the amorphous Ti implanted layer contributed additional toughness to the Co-based matrix, thereby delaying brittle fracture damage to this phase. A corresponding increase in wear resistance of the carbides was not indicated; a consequence, perhaps, of recrystallization softening during implantation. This is consistent with the results of the LMPI samples friction study (15), discussed in a previous section, which showed increased surface damage to the carbide particles following high fluence Ti implantation. Apparently, then, the superior wear resistance of the Ti implanted surfaces can be attributed only to the matrix phase implant layer. The enhanced cohesion at carbide-matrix interfaces observed on eroded Ti implanted surfaces suggests that these regions also play an important role in determining alloy erosion and abrasion resistance. Further study is needed to fully characterize the chemistry and structure of the interface regions and their influence on the early stages of wear.

Work is continuing to determine the implantation depth in the alloy as well as the extent of the amorphous layer. No attempt was made in this study to determine the minimum Ti ion fluence or energy neccessary to drive the surface amorphous, or to correlate improved tribological behavior with a critical surface concentration of carbon. Neither has the role of carbon

-9-

in the stabilization of the disordered phase been identified. These topics remain to be addressed in more extensive studies.

After N implantation the dominant microstructural change observed in the alloy was the extremely high stacking fault density in the matrix phase. The origen of this particular feature; i.e., whether due to implantation induced damage, or to the presence of N in the alloy lattice, or both , is unclear. Neither is a complete explanation of the effects of N on the alloy tribology yet available. Since the metastable fcc phase was found in both nonimplanted and N implanted alloy foils, the possible role of N as an fcc phase stabilizer cannot be commented on. It is possible that the presence of a greatly increased fault density in the implant layer limited the ability of the alloy to respond plastically under stress, and that this effect, in and by itself, produced the poor abrasion resistance exhibited by the N implanted Stoody 3 surfaces.
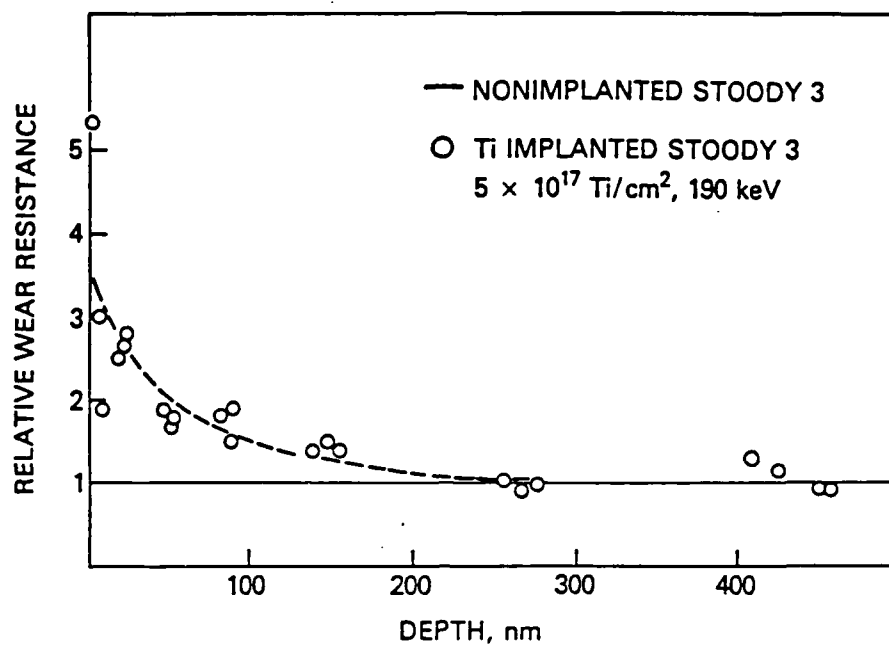
Figure 1a. Relative wear resistance of titanium implanted Stoody 3, abraded with 1-5 micron diamond, vs. depth (Ref. 9).
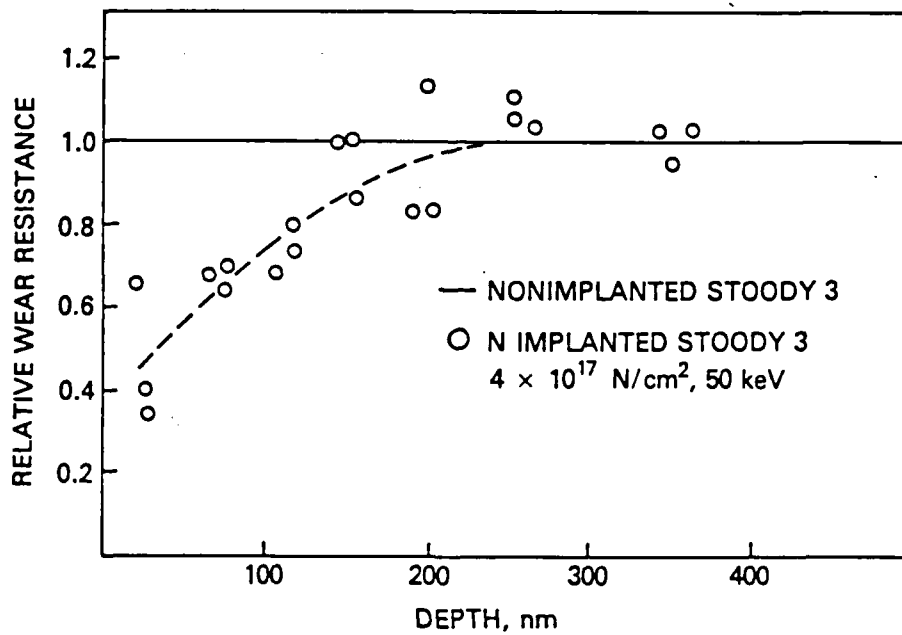

Figure 1b. Relative wear resistance of nitrogen implanted Stoody 3, abraded with 1-5 micron diamond, vs. depth (Ref. 9).
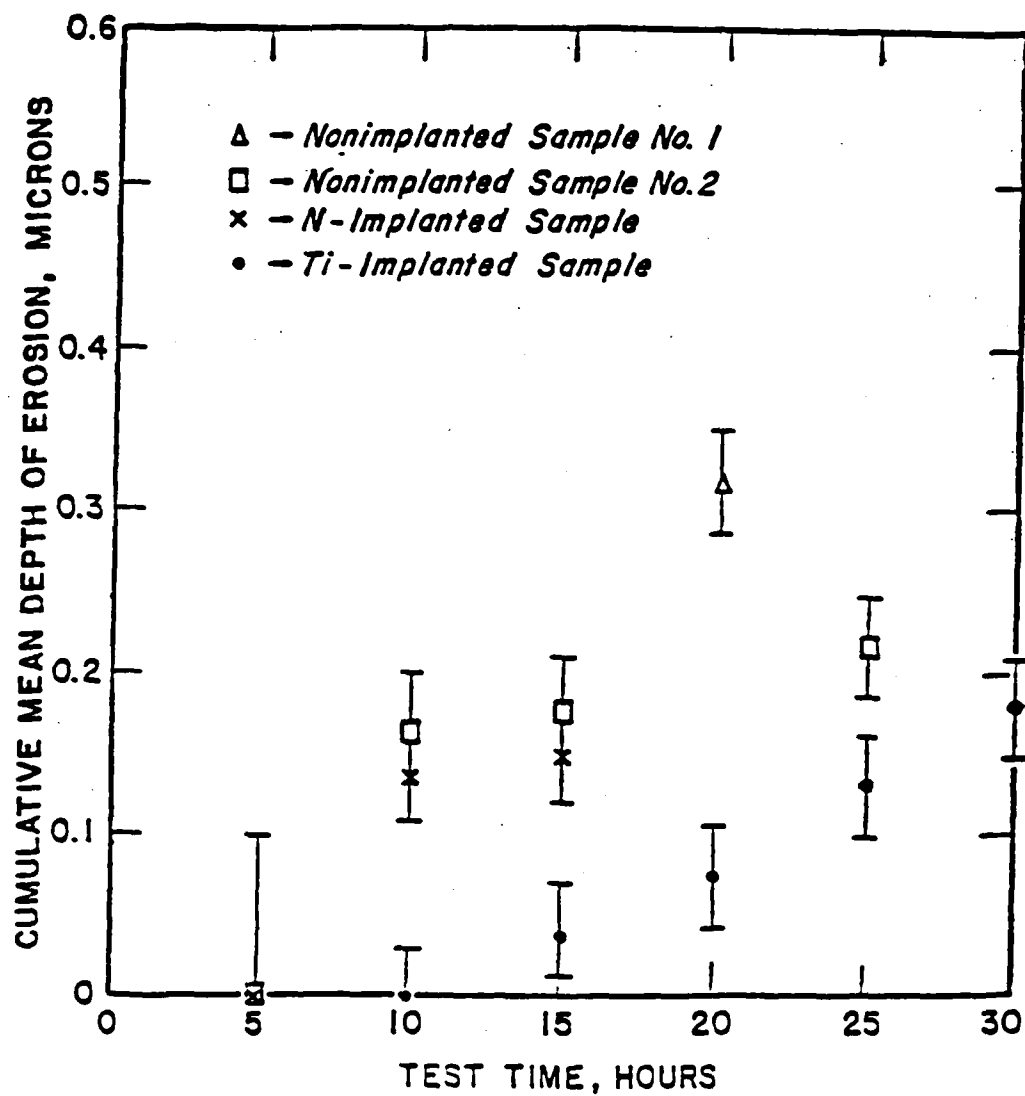
Figure 2. Mean depth of erosion vs. test time for nonimplanted and ion implanted Stoody 3 samples.

Figure 5. Cavitation erosion tested Stoody 3 sample after 3 hours of testing (top) and after 6 hours of testing (bottom).
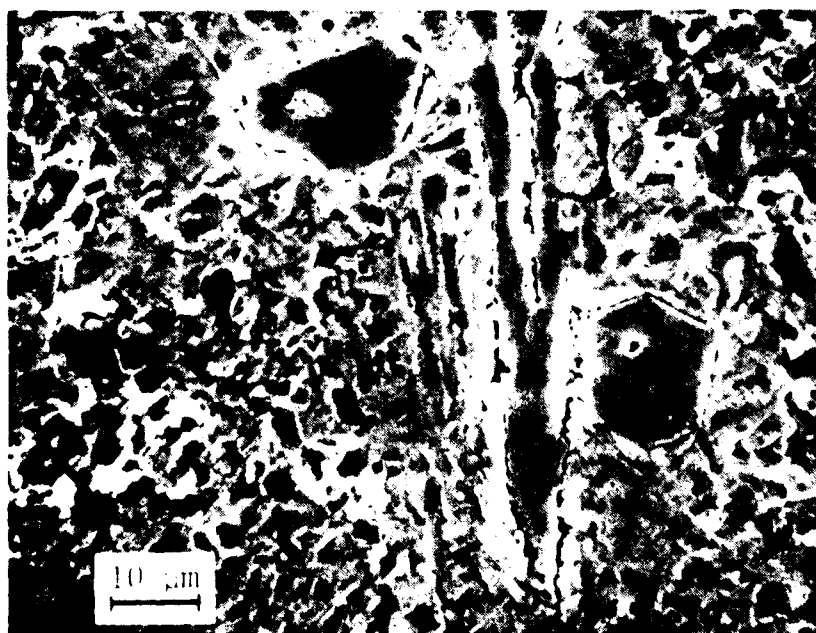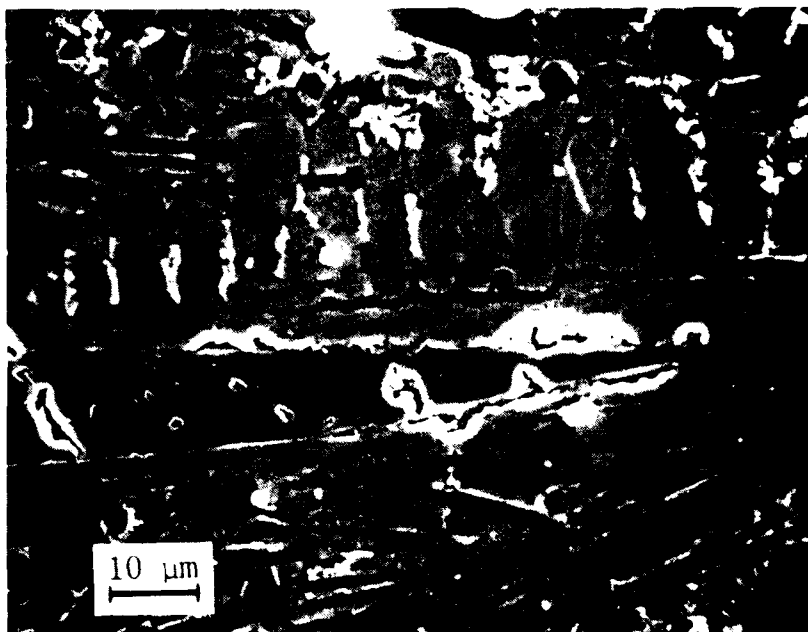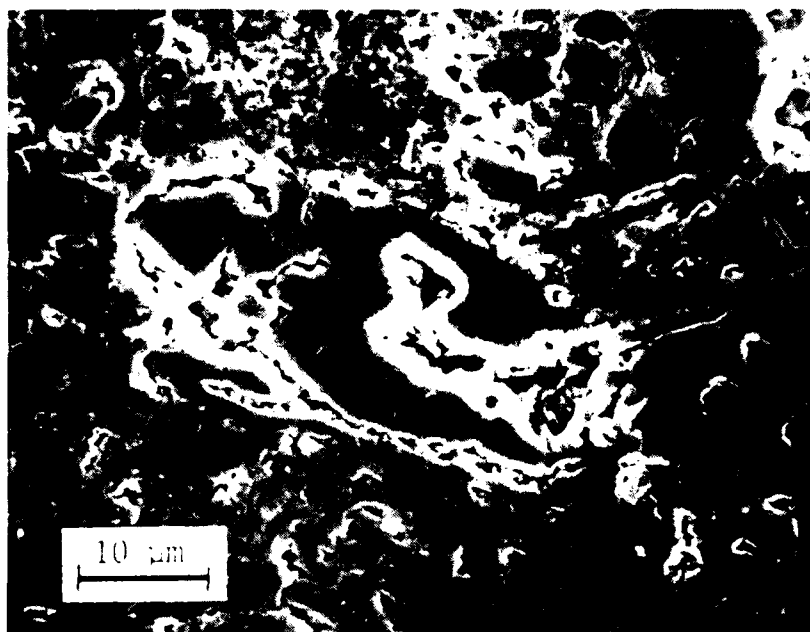
Figure 4. Cavitation erosion tested Stoody 3 sample after
10 hours of testing (top) and after 25 hours
of testing (bottom).
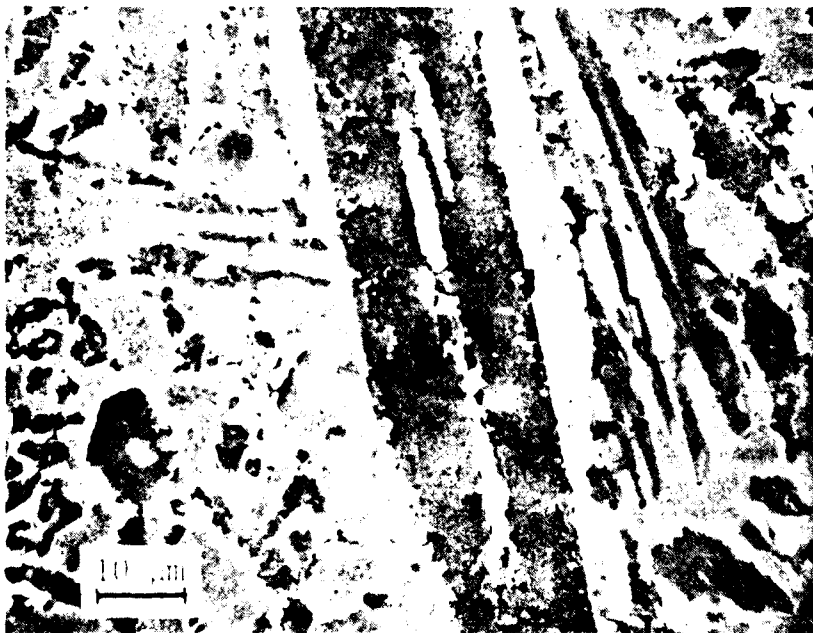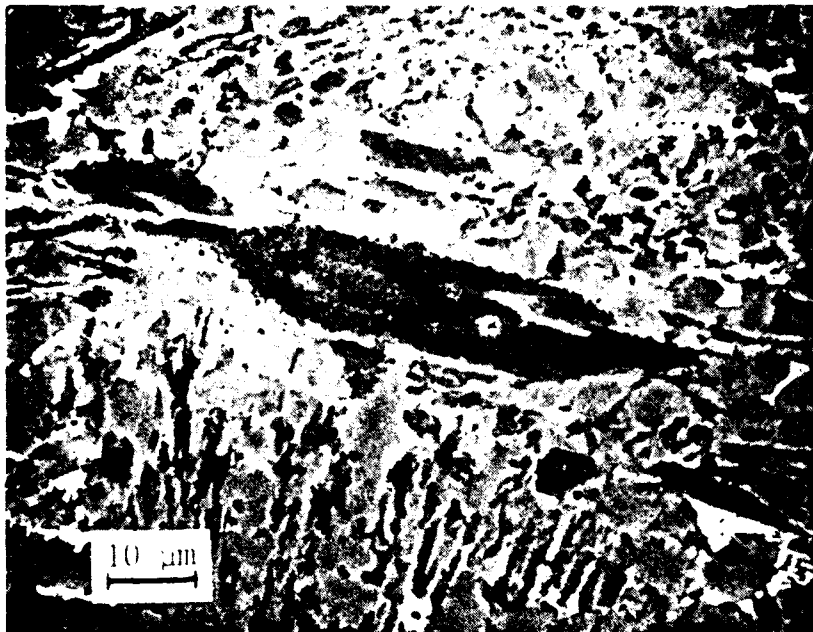
-14-

Figure 5. Cavitation erosion in the microstructure of a
sample after further tests.
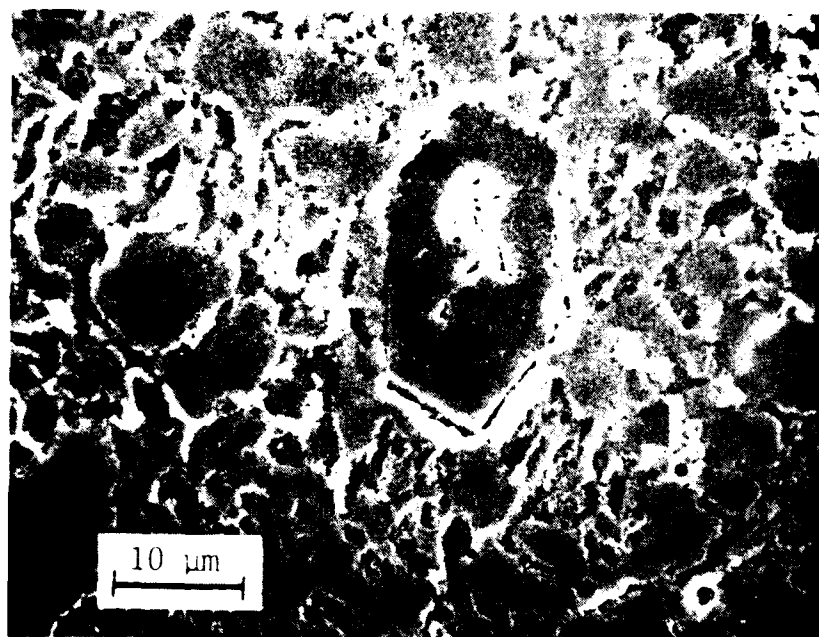
Figure 1. Cavitation erosion tests of explanted fresh 3 specimen before {illegible} and after {illegible}

Figure 1. [illegible caption text]
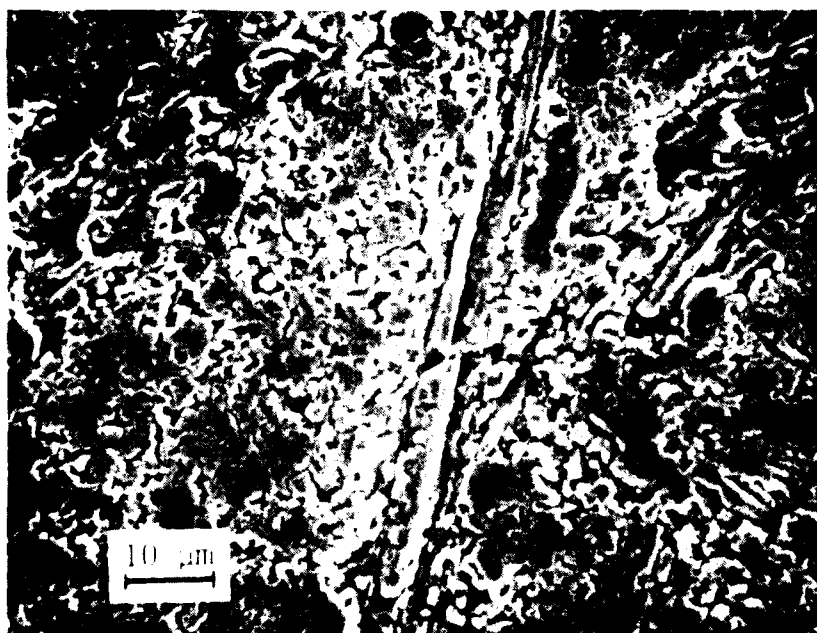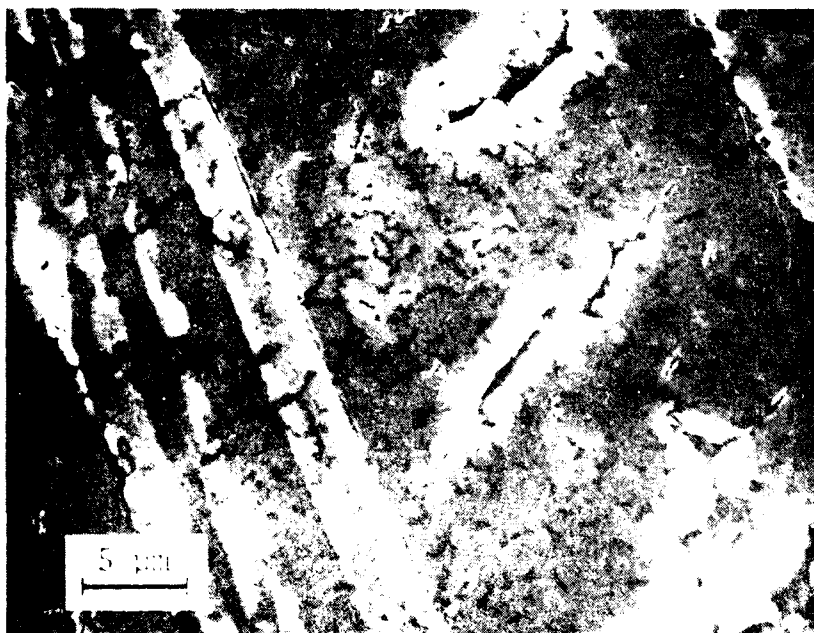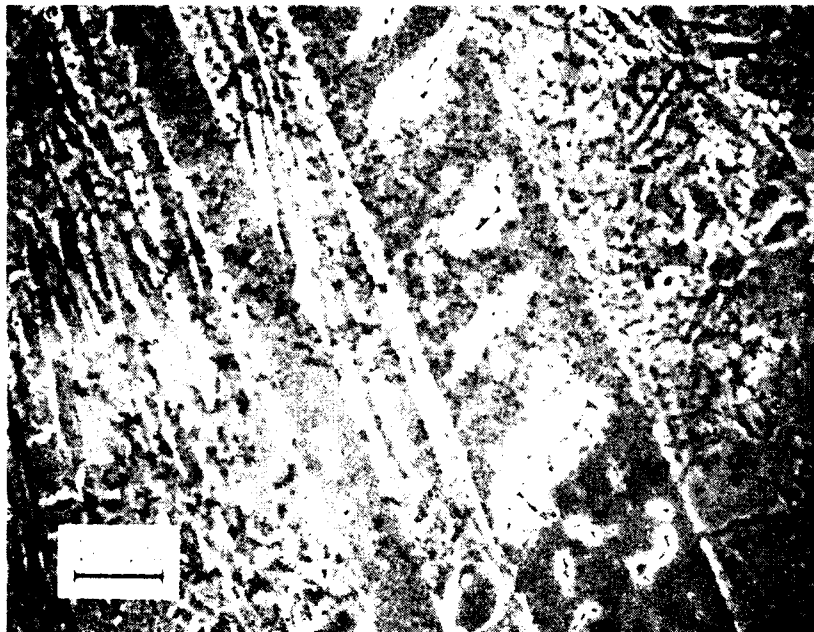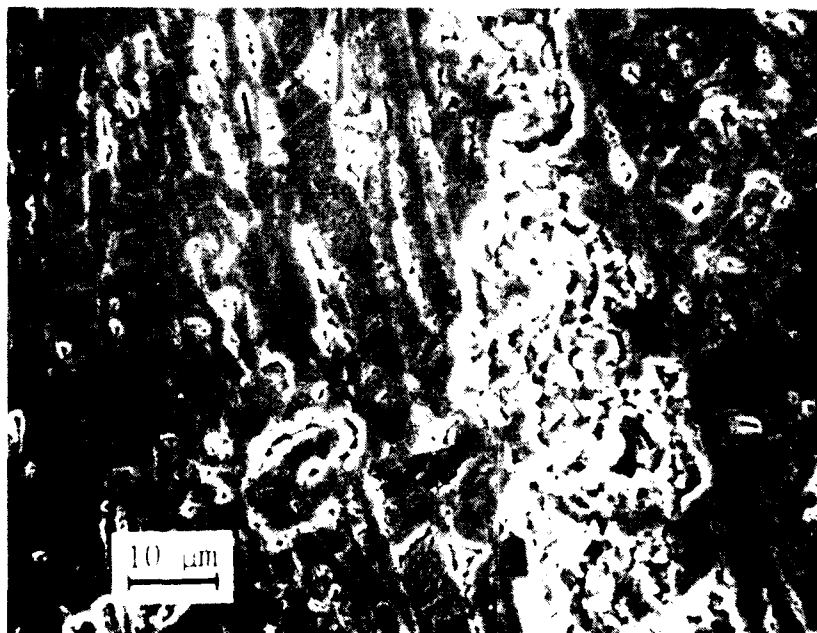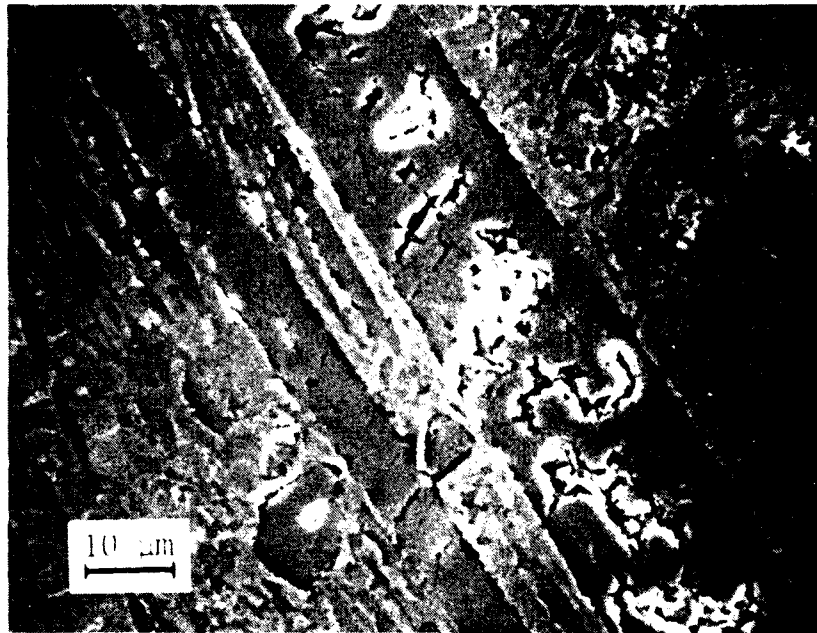
Figure 8. Cavitation erosion tested Ti implanted Stoody 3
          sample after 10 hours of testing (top) and
          after 20 hours of testing (bottom). Photos show
          same region as in Figure 7.
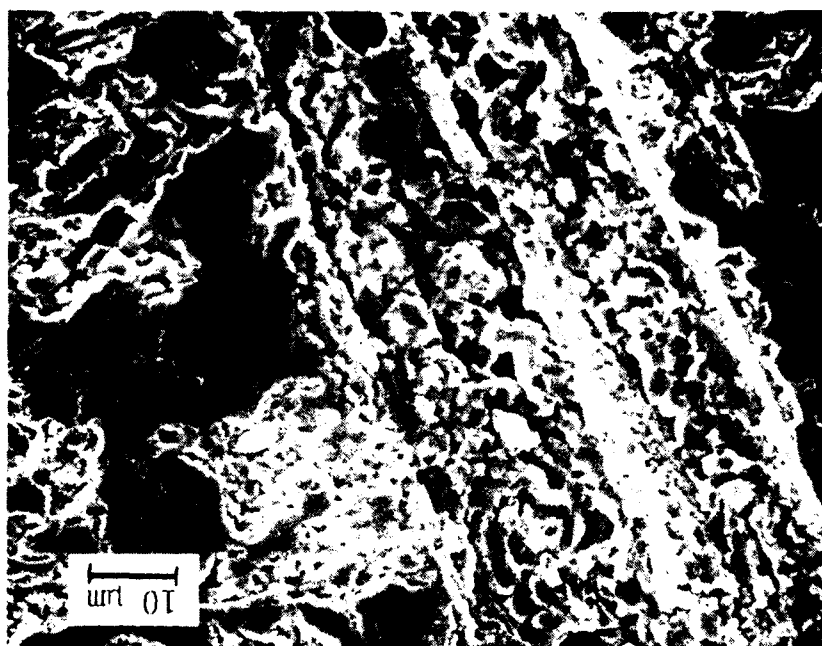
Figure 9. Cavitation erosion tested Ti implanted Stoody 3
sample after 35 hours of testing. Same region
as in Figures 7 & 8.

Figure 10. SEM micrographs of a nonimplanted foil. Several distinct carbide morphologies could be distinguished in the alloy: large dark lath or block shaped carbic a light "script" phase, and smaller light and dark elliptically shaped carbides dispersed between the larger carbides.

Figure 11.   Brightfield micrographs of nonimplanted foils.
             The matrix phase was characterized by networks of
             planer defects running through the grains (top).
             Dislocation tangles were seen, infrequently, in
             combination with the faults or concentrated at the
             grain boundaries (bottom).

-21-

Figure 12. Brightfield micrograph of the matrix phase in a
nonimplanted foil and the corresponding SAD pattern
(110 zone, fcc).

CARBIDE

MATRIX

0.1 μm

Figure 13. Brightfield micrograph of a carbide-matrix
interface with an SAD pattern from the carbide.

-23-

Figure 14. Brightfield micrograph of the matrix phase in an
unpolished foil and the corresponding SAD pattern
(211 zone, fcc).

Figure 15.   Brightfield micrograph of the matrix phase in a Ti
             implanted foil and the corresponding SAD pattern. The
             diffuse rings in the pattern indicated an amorphous
             surface layer in this phase.

-25-

0.1 µm

B
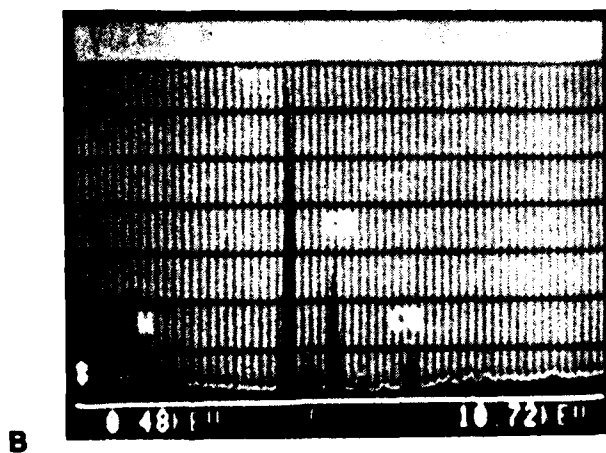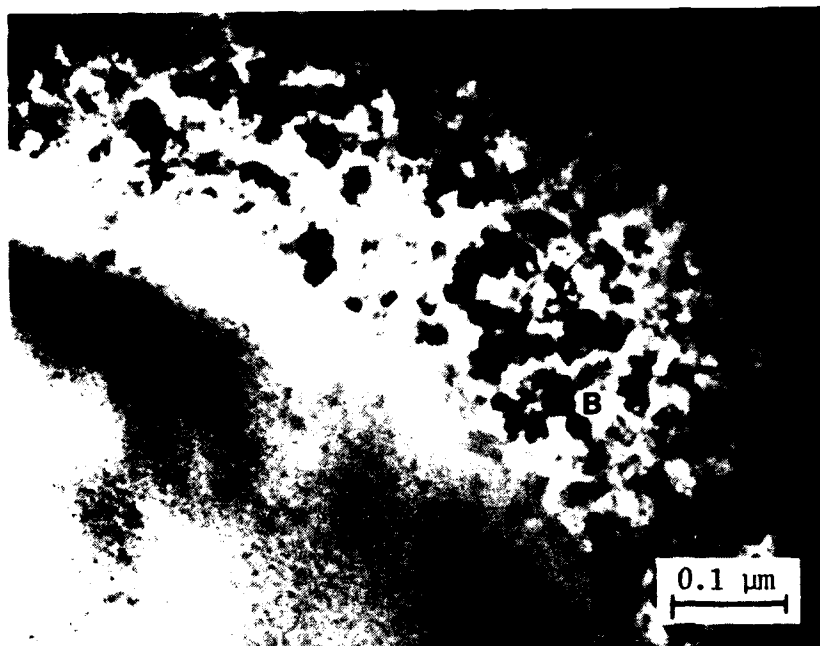
Figure 16. Brightfield micrograph of a) the matrix and
b) a polycrystalline carbide in a Ti implanted foil.
The EDX spectra identifying the polycrystalline phase
as a carbide is also shown.
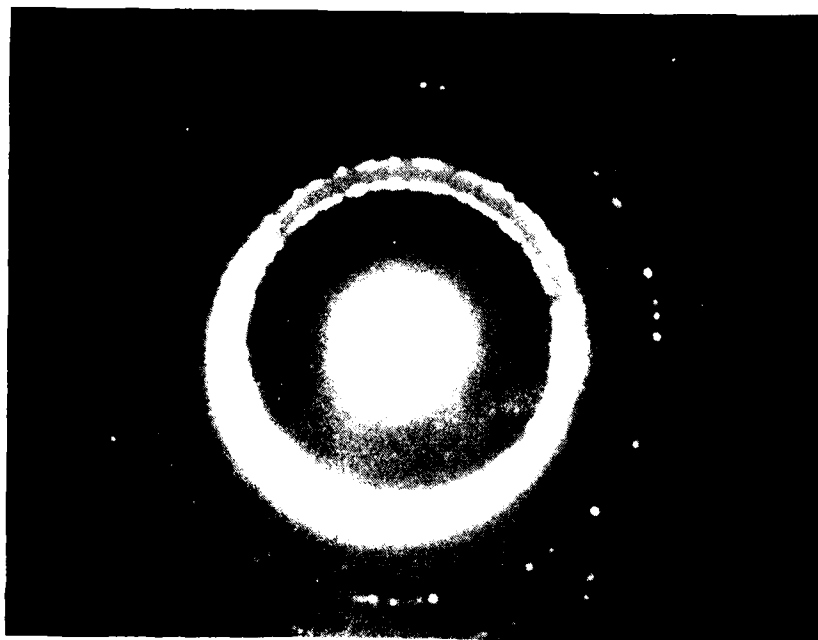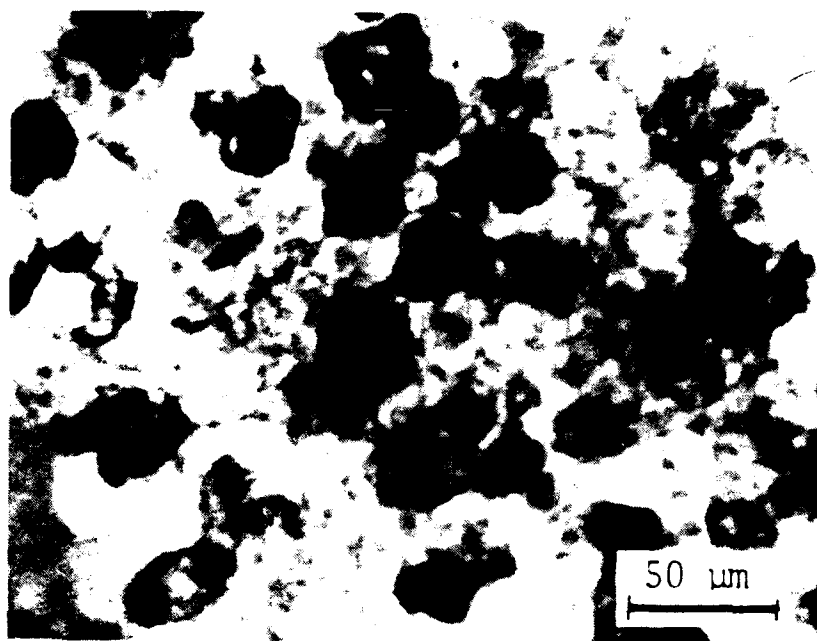
Figure 17. Brightfield micrograph of a carbide in the Ti implanted
foil and the corresponding SAD pattern. The rings in the
pattern indicated a polycrystalline phase. Partial
amorphization of the carbide surface was suggested by the
diffuse nature of the rings.
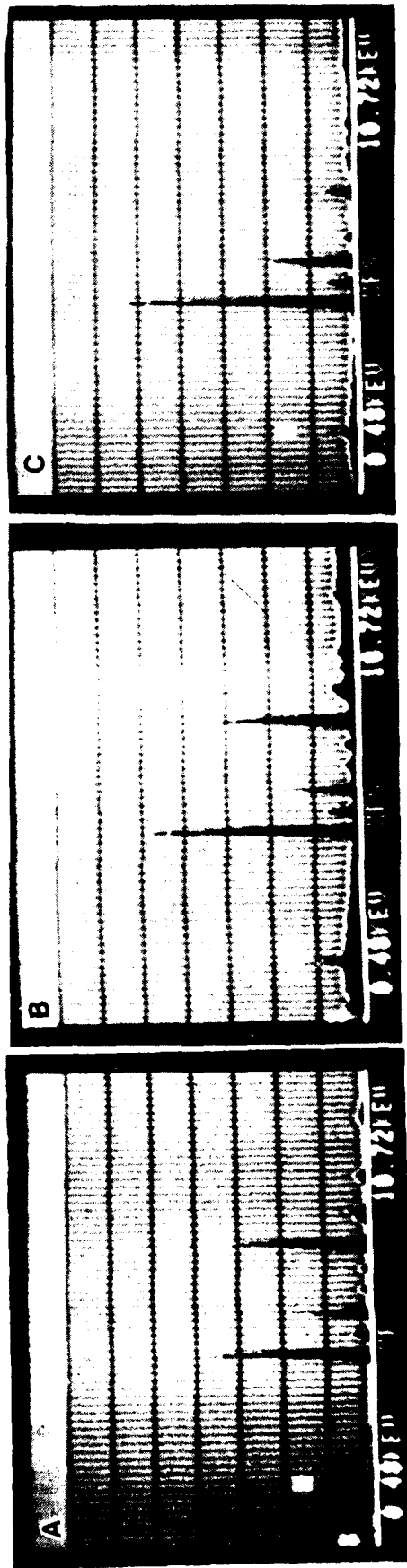
Figure 18. Brightfield micrograph of the Ti implanted foil and EDX spectra from
a) matrix, b) matrix material bordering the carbide and c) carbide.
The matrix appeared to have a lower surface concentration of Ti than
the carbide or bordering matrix material.
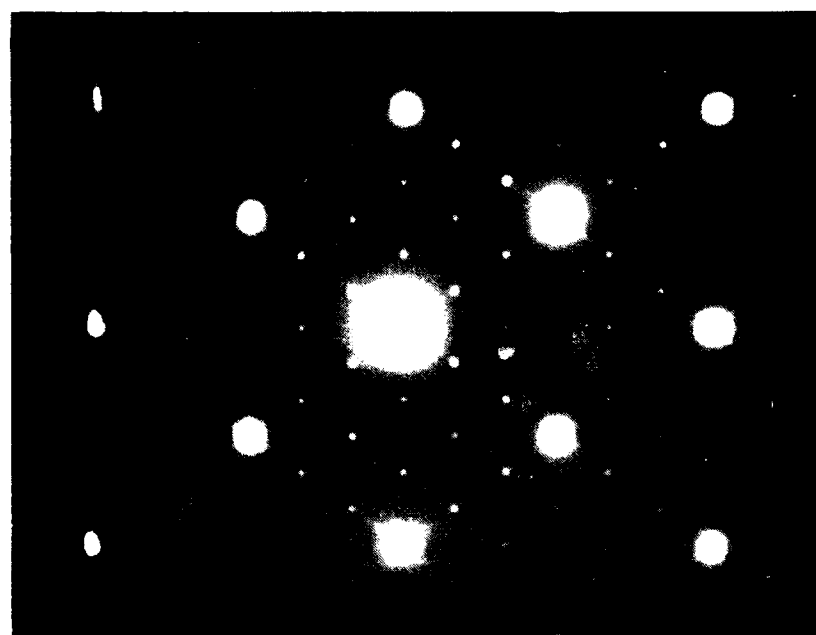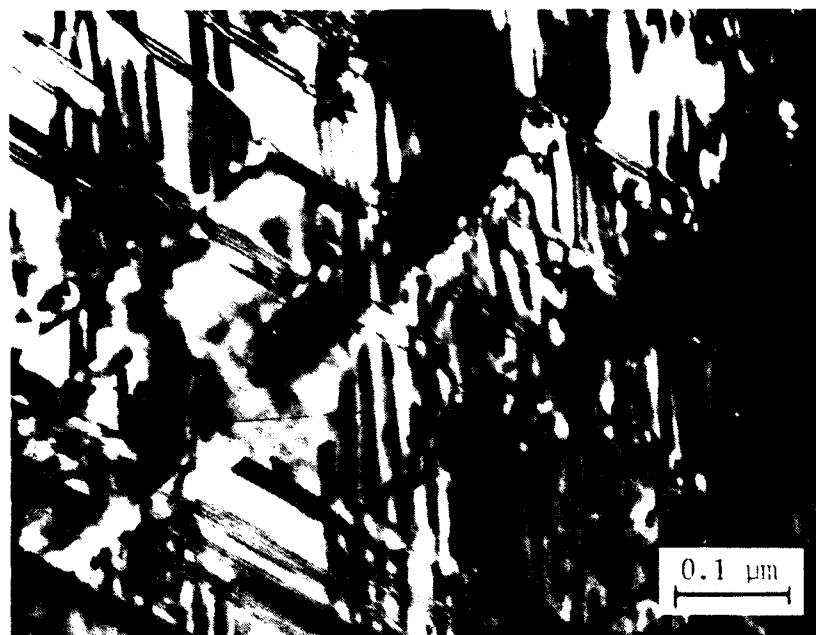
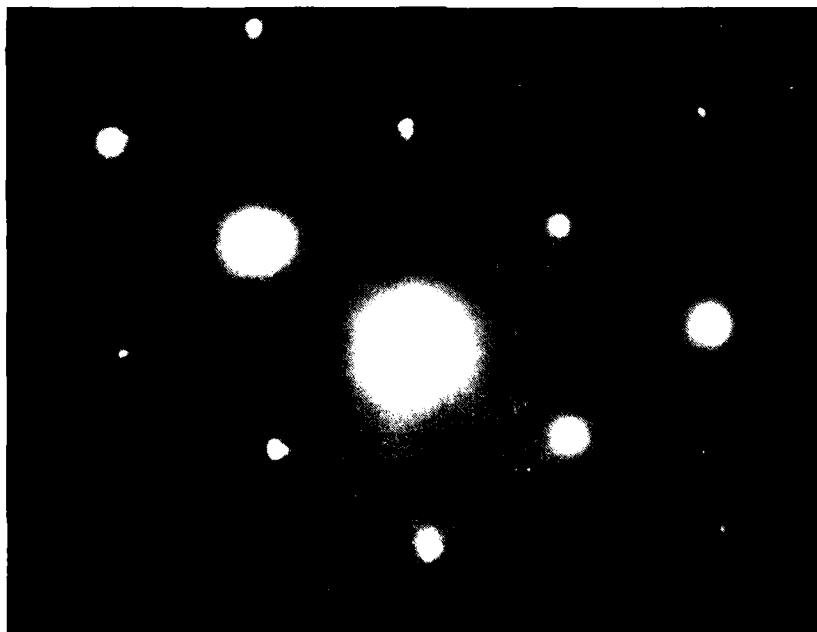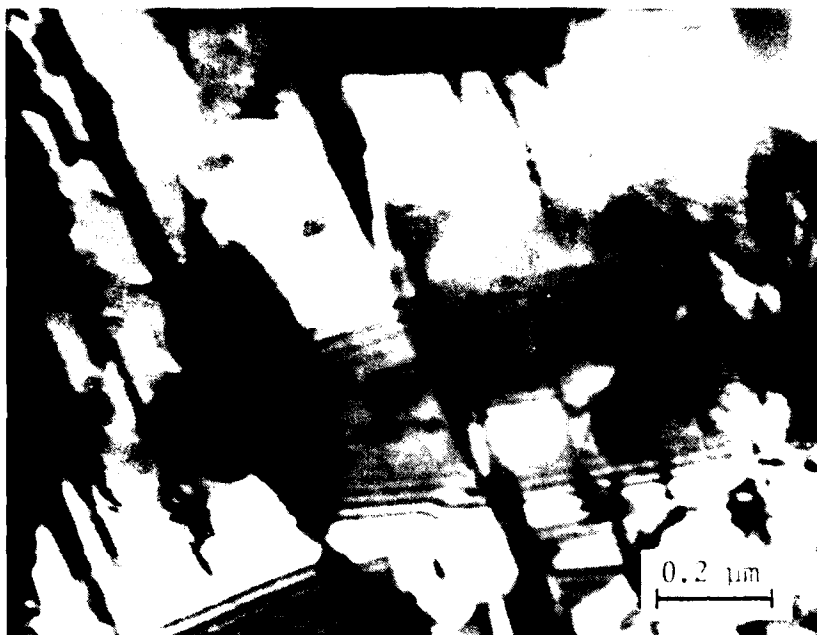Figure 19. Brightfield micrograph of the matrix phase in a N implanted foil and the corresponding SAD pattern (110 zone, fcc). The extra spots grouped in clusters around the basic fcc cobalt spots are believed to originate from carbides dispersed in the matrix.
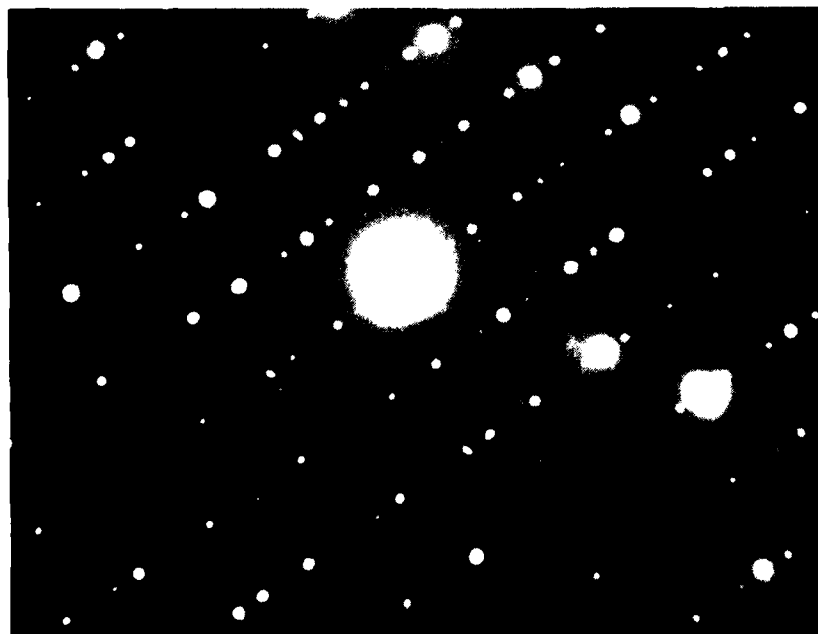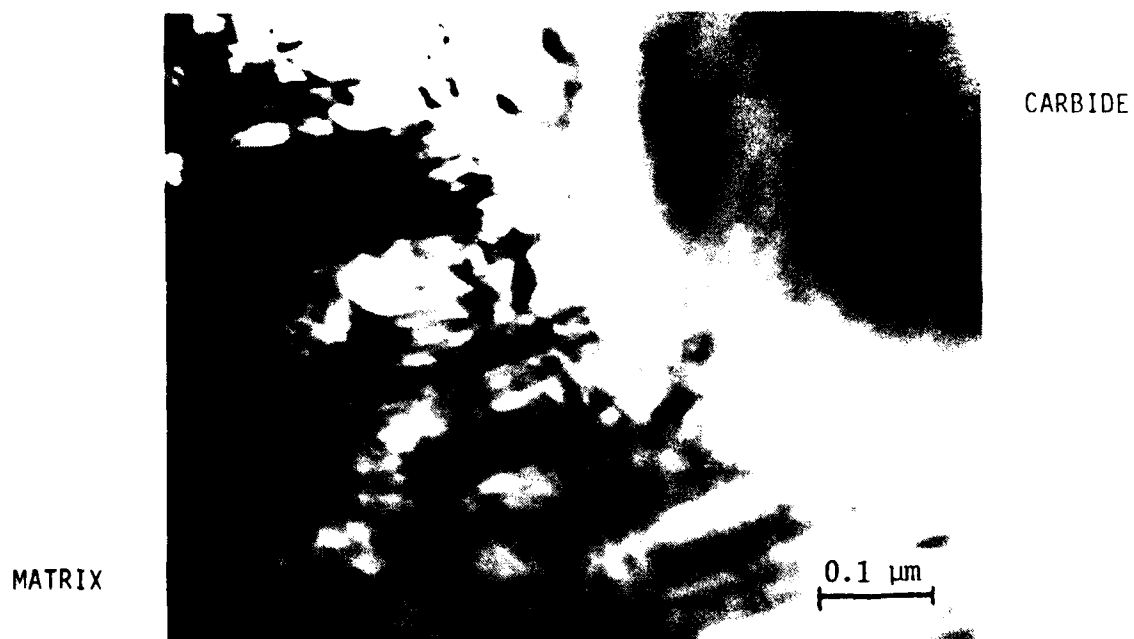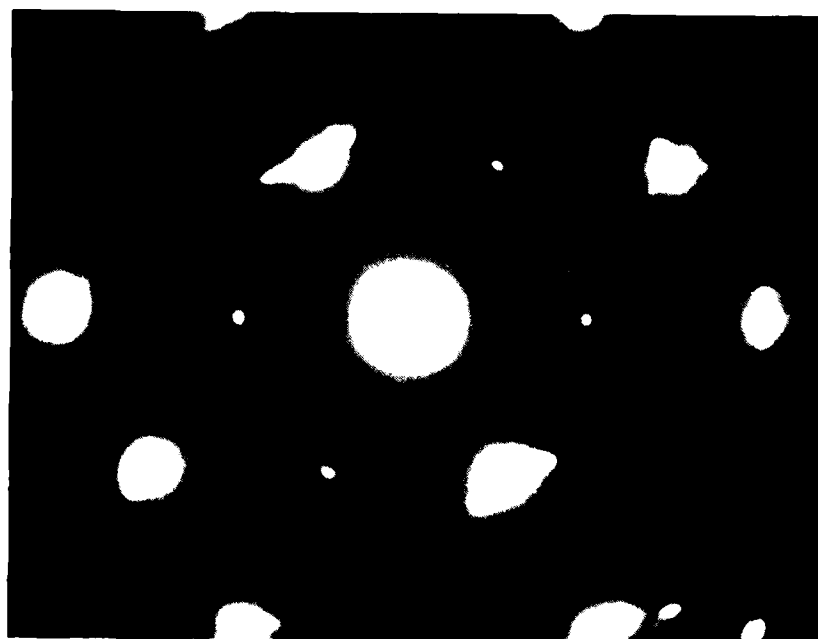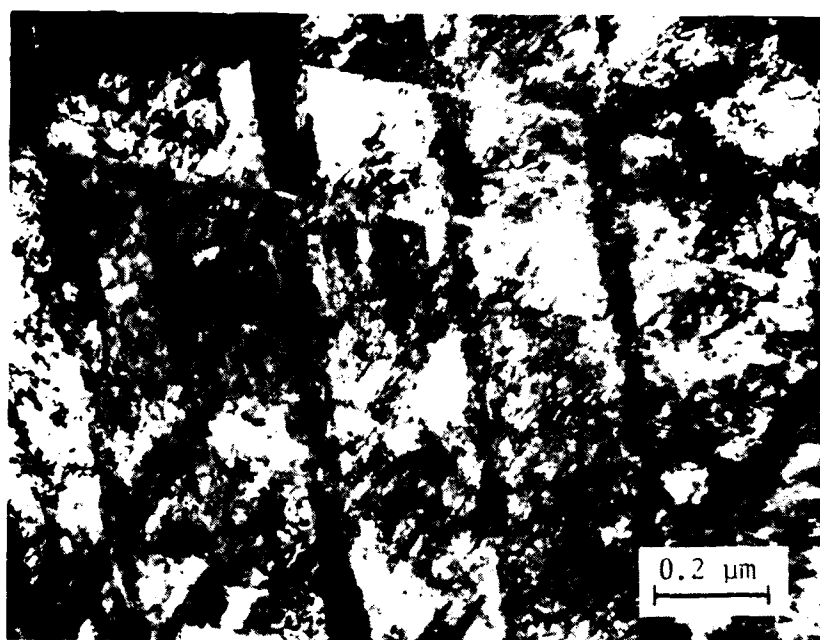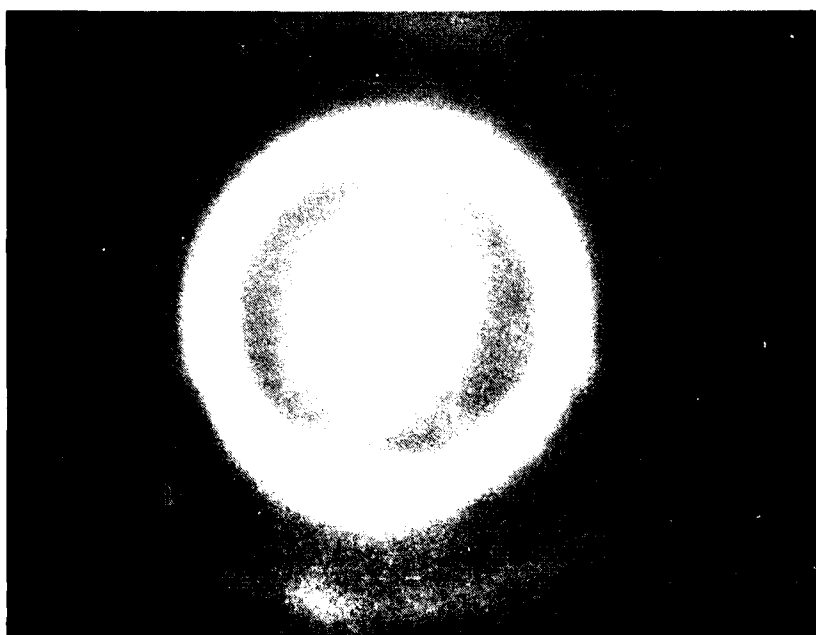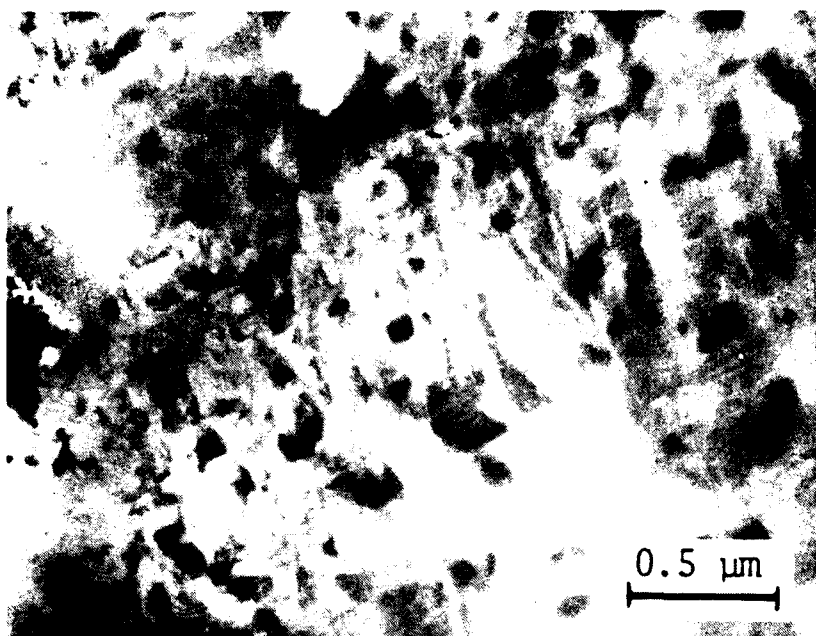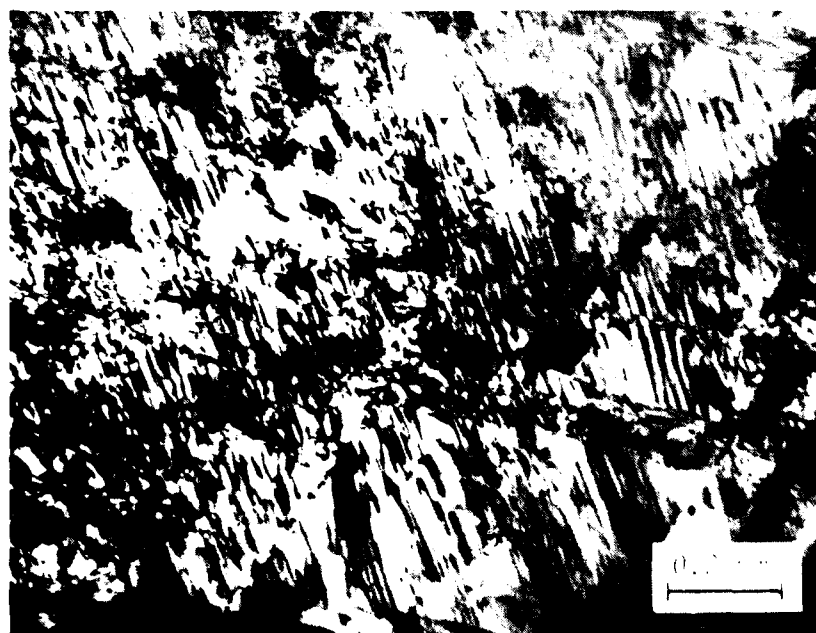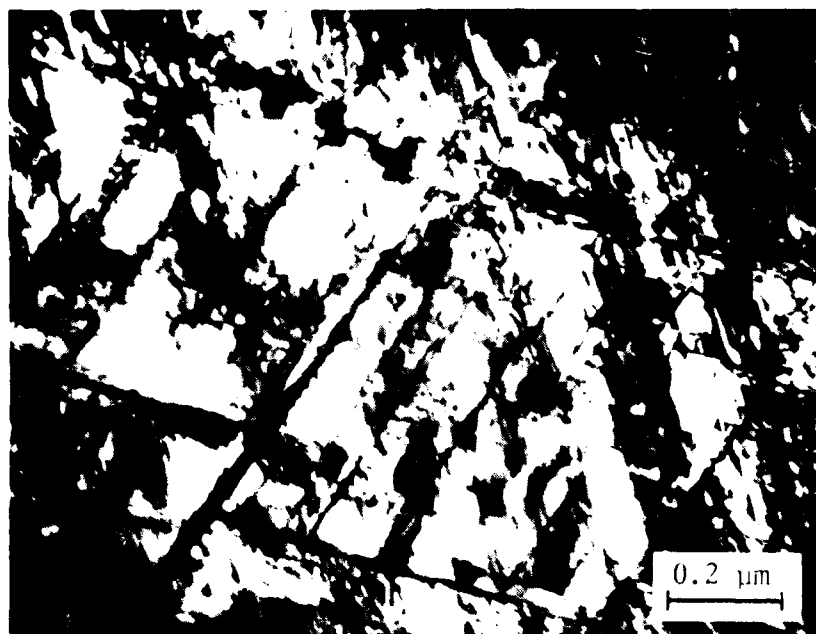
Figure 2. Brightfield micrographs of matrix regions in a
N implanted foil. Very high stacking fault
densities were seen in this phase.

REFERENCES

1. N. E. W. Hartley, in Treatise on Materials Science and Technology, v.18, Ion Implantation, J. K. Hirvonen, ed., Academic Press, N.Y. (1980) 321.

2. I. L. Singer and R. A. Jeffries, J. Vac. Sci. and Technology, A1 (1983) 317.

3. I. L. Singer, in Mat. Res. Soc. Symp. Proc. vol 27, Elsevier, N.Y. (1984) 637.

4. C. Allen, A. Ball and B. E. Protheroe, Wear, 74 (1981-82) 287.

5. K. C. Antony, J. of Metals, (February, 1973) 52.

6. K. J. Bhansali and A. E. Miller, Wear, 75 (1982) 241.

7. S. A. Dillich and I. L. Singer, Thin Solid Films 73 (1981) 219.

8. S. A. Dillich, R. N. Bolster and I. L. Singer, in Surface Engineering, R. Kossowsky and S. C. Singhal eds, NATO ASI Series E, No. 85 (1984) 197.

9. S. A. Dillich, R. N. Bolster and I. L. Singer, Mat. Res. Soc. Symp. Proc. vol. 27 (1984) 637.

10. I. L. Singer, C. A. Carosella and J. R. Reed, Nucl. Instrum. and Methods 182/183 (1981) 923.

11. D. M. Follstaedt, F. G. Yost and L. E. Pope, Mat. Res. Soc. Symp. Proc. vol. 27 (1984) 661.

12. G. Dearnaley, B. James, D. J. Mazey and F. J. Minter, in Proc. Plansee Conf.,Reute, Austria (1985), in press.

13. J. D. Ayers, R. J. Schaefer and W. P. Robey, J. Met. 33(8), (1981)19.

14. J. D. Ayers and R. N. Bolster, Wear 93, (1984) 193.

15. S. A. Dillich and I. L. Singer, in Proc. ASM Intn'l Conf. on Surface Modifications and Coatings, (Oct.1985), in press.

16. C. M. Preece, Treatise on Materials Science and Technology, vol. 16, Cavitation Erosion, (1979) 249.

INDEX OF TECHNICAL REPORTS

End of Fiscal Year Report, submitted to ONR 9/85.

Final Report, submitted to ONR 4/86.

INDEX OF PUBLICATIONS

"Friction and Surface Chemistry of Implantation Modified Metal/Carbide Composites", Sara A. Dillich and Irwin L. Singer, Proc. ASM's International Conference on Surface Modifications and Coatings, October 1985, in press. Also to be published in Surface Films and Coatings.

Submitted for presentation at the 1986 Conference on Surface Modifications of Materials by Ion Beams, July 1986, Ontario, Canada (proceedings to be published in Journal of Materials Science):

"Effects of Ti Implantation on Cavitation Erosion of Co-Based Metal/Carbide Systems", N. V. H. Gately and S. A. Dillich

"Structural Changes in a Co-Based Alloy After High Fluence Ion Implantation", S. A. Dillich and R. R. Biederman

Metals/Materials Technology Series

FRICTION AND SURFACE CHEMISTRY OF IMPLANTATION MODIFIED METAL/CARBIDE COMPOSITES

Sara A. Dillich
Worcester Polytechnic Institute
Worcester, Massachusetts

Irwin L. Singer
Naval Research Laboratory
Washington, D.C.

8512-023

8512-023

FRICTION AND SURFACE CHEMISTRY OF IMPLANTATION MODIFIED METAL/CARBIDE COMPOSITES

Sara A. Dillich
Worcester Polytechnic Institute
Worcester, Massachusetts
Irwin L. Singer
Naval Research Laboratory
Washington, D.C.

ABSTRACT

Dry sliding friction measurements were performed on model carbide/metal composite samples containing 24 to 42 volume % carbide. Wear debris, located preferentially on the carbides, were analysed using SEM/EDX and Auger Scanning Microscopy (SAM). The friction and wear of the composite samples were found to be influenced by the compatibility (degree of mutual solubility) of the carbides with the steel counterface, as well as by local inhomogeneities in the carbide distribution. Friction tests were also made on the samples following high fluence Ti implantation. Implantation resulted in increased friction and wear, possibly due to an implantation induced softening or degradation of the carbides.

CARBIDE STRENGTHENED ALLOYS, (e.g., Stellite alloys, tool steels, 440C steel) are valuable wear resistant materials. The carbides provide high hardness to the alloys, but little else is known about their influence on friction or on initial wear and transfer film formation. The intent of this study was to identify the role of the carbide phases in the friction and wear behavior of carbide-strengthened alloys. To this end, low speed, dry sliding friction measurements were made on model carbide/metal matrix composites tested against 52100 steel, followed by light and electron microscope examinations of the wear scars.

From previous analyses of commercially available composites (e.g. a Co-based superalloy, Stoody 3) it was realized that carbide/metal matrix microstructures are, in general, too fine to easily distinguish the tribological effects of different phases. For this reason, carbide/metal matrix composites formed by a new surface processing technique, the Laser Melt Particle Injection process (LMPI), were used in this study.

The composite surfaces were prepared at the Naval Research Laboratory by injection of TiC and WC particles into Ti or Al alloy surfaces (1,2). These LMPI surfaces offer a unique opportunity for the investigatin of dry sliding friction and wear of transition metal/carbide composite surfaces. The large sizes of the carbides (on the order of 100 microns) allow easy identification of separate phases with both light and electron microscopes. Chemical profiling of debris and microwelds on friction tested surfaces are possible using high resolution scanning auger microscopy (SAM) in conjunction with ion sputtering. This cannot be easily performed on conventional metal-carbide composites (e.g. superalloys and cemented carbides) for which the carbides are typically an order of magnitude or more smaller. Thus, specific contributions of the carbide and matrix phases to the galling friction and wear of an alloy system can be investigated by taking advantage of the "magnified picture" provided by the LMPI samples.

Ion implantation is another surface modification technique which has been found to improve the tribology of engineering alloys (3-5). Because of the extreme shallowness of the implant depths (≈100-200 nanometers), implantation can also be used as a research tool, to assist in the determination of controlling wear modes operative at the surface during the initial stages of wear. High fluence Ti implantation was also successful in reducing friction and wear of a Co-based superalloy (6). However, the influence of implantation on the separate phases of metal/carbide alloy systems with conventionally sized carbides is not easily deduced. To aid in this determination, and in the characterization of the tribology of the steel - metal/carbide couples, friction tests were also made on the LMPI samples after high fluence Ti implantation.

EXPERIMENTAL PROCEDURE

A description of the laser processing technique and equipment can be found in References (1&2). Disks 1.27 cm. in diameter by 0.27 cm. thick were cut from carbide injected plates. Before testing, the surfaces were diamond polished to a 1 micron finish and cleaned with organic solvents. The matrix alloy compositions, as well as carbide types, sizes, and average volume fractions, of the test disks are listed in Table I.

Friction measurements were made in ambient air (40% - 60% humidity, room temperatures) using a ball on disk test geometry. The stationary balls (AISI 52100 steel, 1.27 cm. diameter) made contact with the moving LMPI disks. A sliding velocity of 0.1 mm/sec was used, with an applied normal load of 9.8 N. Except when noted, tests consisted of 20 unidirectional passes of a ball on a disk. The first pass of each test was 5 mm in length, while subsequent passes over the same track were 3 mm long. The applied normal load and the tangential frictional forces during testing were monitored continuously on a dual trace chart recorder. The coefficient of kinetic friction, μ_k, was calculated for each pass as the ratio of the tangential force to the normal force and may be considered constant ($\pm$ 25%) unless stickslip (i.e., large amplitude oscillations in the tangential force) is noted.

Polished LMPI disks were implanted in a modified Model 200-20A2F Varion/Extrion ion implanter with a hot cathode arc discharge type ion source. The samples were mounted onto a water cooled holder and the target chamber was cryogenically pumped to pressures of about 3×10^{-6} Torr or better. The disks were implanted with Ti ions at either a) 190 keV beam energy to a fluence of 5×10^{17} Ti/cm^2 or b) 100 keV beam energy to a fluence of 6×10^{17} Ti/cm^2.

Wear tracks on the disks were examined using Scanning Electron Microscopy (SEM) and light microscopy with Differential Interference Contrast (DIC). The elemental compositions of debris in the tracks and on the balls were examined by Energy Dispersive X-Ray analysis (EDX) using a JSM-U3 SEM equipped with a Kevex spectrometer. Composition versus depth profiles of worn surfaces were performed with two different Auger microprobes: one, a Perkin Elmer (PHI) model 600 microprobe, the other with a model 590 microprobe. Auger derivative spectra were taken with electron beam voltage at V = 2kV and modulation amplitude at V = 3 or 6 eV. Depth profiles were recorded during ion milling with a rastered 2 keV Ar ion beam.

RESULTS

A summary of the dry sliding friction coefficients, μ_k, and the EDX analysis of the wear debris on 1 and 20 pass tracks is shown in Tables II & III for nonimplanted and implanted surfaces, respectively. A range of values, instead of a single average value, listed for a friction coefficient in Table II & III denotes the occurrence of stickslip. EDX analysis of debris on ball scars from selected 20 pass tracks is summarized in Table IV.

FRICTION - In general, the nonimplanted disks showed lower μ_k values than did the implanted disks. The lowest friction coefficients ($\mu_k \simeq 0.2$) after 20 passes were observed on the TiC/Ti sample 80-5). The WC/Ti disks on the other hand, exhibited

Table I - Carbide Types, Sizes and Volume Fractions in Alloys Tested

Disk #	Alloy	Carbide Type	Size (μm)	Volume* %
80-5	Ti-6Al-4V	TiC	105-210	36 ± 2
80-20	"	WC	105-149	24 ± 4
80-21	"	WC	105-149	37 ± 5
80-31	6061 Al	TiC	74-88	31 ± 6
80-32	6061 Al	TiC	74-88	42 ± 5

* average values, from Ref. 2

Table II - Coeff. of Friction and Wear Debris Analysis for AISI 52100 Balls Sliding Against Laser Processed Disks

Sample #	Test #	1st pass	Debris*	20th pass	Debris*
80-5	1	0.16	no	0.25	no
TiC/Ti	2	0.18	no	0.18	no
	3	0.15	no	0.24	no
80-20	1	0.23	no	.08-.42	Ti,Fe
WC/Ti	2	0.21	no	.20-.56	"
	3	0.20	no	.16-.44	"
80-21	1	0.23	no	0.41	no
WC-Ti	2	0.16	no	0.46	no
	3	0.18	no	0.43	no
80-31	1	0.17	no	0.25	no
TiC/Al	2	0.18	no	.20-.38	Al,Fe
80-32	1	0.18	no	0.36	no
TiC/Al	2	0.18	no	0.35	no

* Identified by Energy Dispersive X-Ray analysis (EDX)

2

Table III - Coefficients of Friction and Wear Debris Analysis for AISI
52100 Balls Sliding Against Laser Processed Disks Implanted with Ti

Sample #	Implant[+]	Test #	1st pass	Debris*	20th pass	Debris*
80-5	a	1	.28-.56	Ti,Fe	0.35	Ti,Fe
TiC/Ti		2	.20-.52	"	0.34	"
	b	1	0.28	Ti,Fe	0.39	Ti,Fe
		2	0.24	"	0.38	"
		3	0.24	"	0.29[c]	"
80-20	b	1	.30-.60	Ti,Fe	0.30[d]	Ti,Fe
WC/Ti		2	0.42	"	.22-.48	"
		3	0.48	"	.32-.56	"
80-21	a	1	0.42	Ti,Fe	.12-.42	Ti,Fe
WC/Ti		2	0.48	"	.14-.46	"
80-31	b	1	0.32	Al,Fe,Ti	.20-.38	Al,Fe,Ti
TiC/Al		2	0.31	"	.20-.48	"
		3	0.33	"	0.36[c]	"
80-32	a	1	0.45	Al,Fe,Ti	.22-.50	Al,Fe,Ti
TiC/Al		2	0.42	"	.20-.50	"

+ a: 5×10^{17} Ti/cm^2 at 190 keV, b: 6×10^{17} Ti/cm^2 at 100 keV
* identified by Energy Dispersive X-Ray analysis (EDX)
c after 7 passes; d after 3 passes

much higher friction ($\mu_k \approx 0.45$), roughly twice as high as the TiC/Ti disk. The disk with the lowest carbide fraction (80-20, 24-4% WC) exhibited stickslip behavior as well. Intermediate values of friction coefficients ($\mu_k \approx 0.35$) were measured on the TiC/Al disks.

Ti implantation produced an increase in the μ_k values for each of the LMPI disks. Also, stickslip occurred earlier and more frequently during testing.

WEAR SCAR AND DEBRIS ANALYSIS - The majority of wear tracks on the nonimplanted surfaces could not be seen by either DIC or SEM microscopy. That is, no damage to the surfaces or debris particles could be detected. One exception was the low carbide WC/Ti disk, 80-20, which showed fine grooves in the Ti-6Al-4V matrix and wear debris along the tracks. Fig. 1 shows a portion of a 20 pass track covered by smeared wear debris. This debris, which is rich in Ti according to EDX analysis (Table II), must have been transferred from the matrix to the ball, then transferred to the carbides when they passed under the ball.

The effects of local variations in carbide concentrations on wear behavior were also seen during tests on the TiC/Al disk, 80-31. Although the average carbide volume for this sample was measured as 31 - 6%, test #2 was made in a track containing only 24 - 2% concentration (as revealed during DIC examination of the track), indicating that contact occurred primarily between the 52100 ball and the Al matrix phase. The wear track for test #2 contained debris which EDX analysis identified as rich in Al

and Fe. In contrast, no wear scar or debris was observed in test #1 on the same disk, for which the local carbide concentration was higher (36 - 2%) than the average value for the disk.

After implantation, all tracks made on the disks were clearly visible. In addition, wear debris containing Fe (from the steel ball) was found in the first pass track on each of the implanted disks (Table III). An illustration of debris on the single pass track of test #1 on WC/Ti disk 80-20 is seen in Fig. 2, which shows large debris fragments attached to carbides. Another example is the 20 pass track on disk
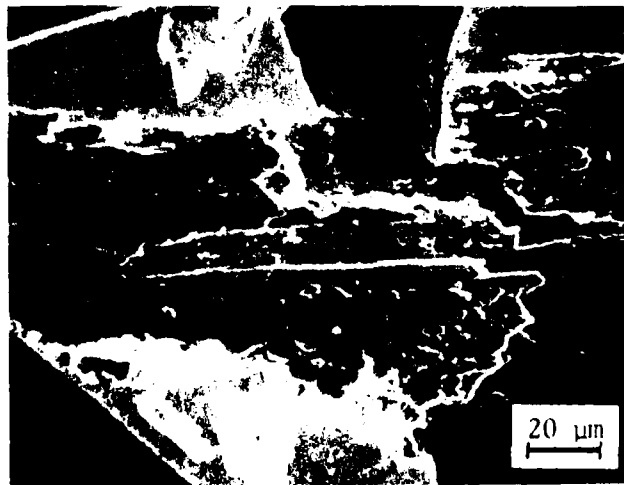

Fig. 1 - Wear track on nonimplanted WC/Ti disk, 80-20, 20 pass region

3

Fig. 2 - Debris on test track #1 on WC/Ti disk 80-20 after Ti implantation, one pass region.

Fig. 3 - Wear track on WC/Ti disk 80-21 after Ti implantation, 20 pass region

80-21, shown in Fig. 3, illustrating the plowing damage deformation to the matrix phase. The Ti implanted TiC/Ti disk, 80-5, was the least degraded by wear. Although considerable debris was generated and deposited on the carbides, the matrix phase of this surface appeared undamaged (Fig. 4, left). The carbides in the implanted disk showed more damage after wear than in the nonimplanted disk. As seen in the DIC micrograph in Fig. 4 (right), sliding produced grooves in the TiC particles. Even more severe damage to the carbides was observed on the other implanted disks. Occasionally, carbide particles in the implanted tracks appeared to have been fractured and fragmented during testing, permitting fine carbide debris to be distributed in some of the tracks (Fig. 3).

Although no damage nor debris could be found on the majority of the nonimplanted tracks, SEM/EDX analysis of wear scars on the corresponding 52100 ball surfaces found evidence of some material transfer to the balls during testing (Table IV). For example, scars on the balls run against the nonimplanted TiC/Ti sample, 80-5 were detectable only by a slight discoloration. Nevertheless, the EDX spot analysis of the ball track indicated the presence of Ti. Similarly, inspection of the ball scar formed against the TiC/Al disk 80-32 showed both Ti and Al. In the case of the balls tested against the high carbide volume WC/Ti disk, 80-21, EDX showed a large W signal (See Fig. 5), indicating that particles from the WC phase adhered and transferred to the ball surfaces. In all cases much larger amounts of debris material were found on ball scars formed against implanted disks. The debris again consisted of an amalgam of disk and ball materials, as well as implanted Ti.

Fig. 4 - 20 pass regions of wear tracks on Ti implanted TiC/Ti disk, 80-5
Left: SEM micrograph   Right: DIC micrograph

4

Table IV - EDX Analysis of Wear Debris on AISI 52100 Steel Balls

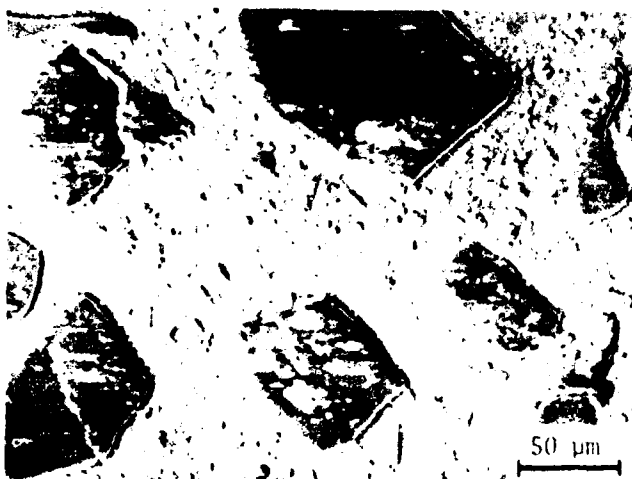| Counter Surface	Implanted	# of Scars Examined	Debris
TiC/Ti (80-5)	NO	2	Fe,Ti
TiC/Ti (80-5)	YES	3	Fe,Ti
WC/Ti (80-21)	NO	2	Fe,W,Ti
TiC/Al (80-31)	NO	1	Fe,Ti,Al
TiC/Al (80-32)	NO	2	Fe,Ti,Al

AUGER ANALYSIS - Auger sputter depth profiles of a portion of the 20 pass wear track on the Ti-implanted TiC/Ti disk are presented in Fig. 6. Three features of the track, shown in the circles in the SEM photo, were profiled concurrently during ion milling: a) non-worn Ti alloy matrix (away from the visible dendritic phase); b) a debris flake attached to a TiC particle; and c) a debris-free carbide surface. Both the Ti alloy matrix and the TiC particle showed changes in surface composition as a result of Ti implantation. The Ti alloy was diluted near the surface by O and C, presumably either by implantation mixing of a surface film TiO_xC_y or by implantation induced absorption of C and O from residual gases (7). The TiC acquired a shallow O layer, and as expected, a surface enriched in Ti. The debris particle, as illustrated in Fig. 6b, consisted of an outer layer rich in Fe oxide followed by an increasing proportion of Ti oxide. Both Fe and Ti were found only in an oxidized state, as deduced by the Ti and Fe line spectra; this portion of the d(NE)/dE spectra, obtained after 10 minutes of sputtering, is shown in the inset of Fig. 6b. As debris material was sputtered away,

the underlying Ti-rich TiC surface appeared. Note that the sputter rate was increased after 20 and 40 min., in effect compressing the true depth scale (not shown) by factors of $\simeq 3$ then $\simeq 5$. A second debris flake was profiled at the same time and virtually identical compositions to that of Fig. 6b were obtained.

Auger sputter depth profiles were also obtained from four debris flakes stuck to the ball scar worn against the 20 pass track just analysed. The debris flakes were mixtures of Fe and Ti, and their oxides, but with only 1/3 to 1/2 the amount of O as the debris on the track. Two flakes had nearly equal amounts of Fe and Ti, and two had five times more Fe than Ti. The reduced O content of the debris flakes on the ball scar as compared to the disk track suggest that the debris oxidized after they had transferred to the track.

DISCUSSION

Debris formation on the nonimplanted disks was observed only on those low carbide tracks which also exhibited stickslip friction, i.e., tracks on the WC/Ti disk 80-20 and track #2 on the TiC/Al disk 80-31. This, and the presence of considerable disk material on balls run against the high friction, nonimplanted WC/Ti disks, indicates that the observed friction behavior can be correlated with adhesive interactions and material transfer between the contacts.

By the compatibility criteria, first introduced by Rabinowitz (8,9), friction couples with high compatibility (i.e., a high degree of mutual solid solubility) experience greater friction and wear than do those with a lower degree of compatibility. This may account then, at least partially, for the lower friction coefficients and wear of the TiC/Ti disk relative to the WC/Ti disks. That is, the solubility of WC in bcc Fe is much higher than that of TiC. For this reason, TiC tools used for the high temperature machining of steel show a much
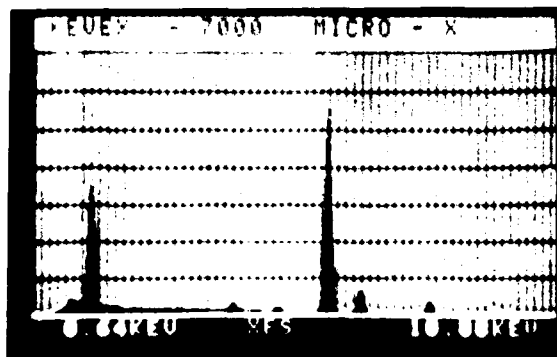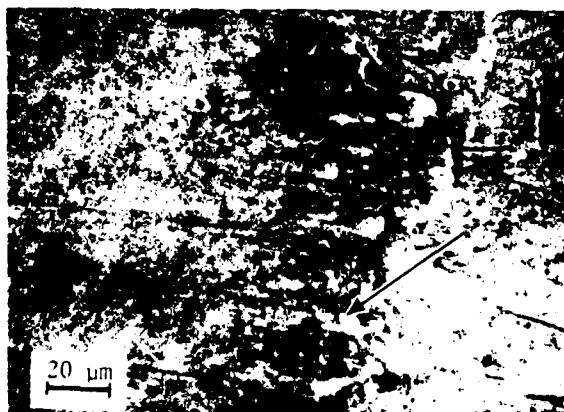
Fig. 5 - Left: Wear scar on steel ball tested against WC/Ti disk Right: EDX signal of a spot on the ball scar
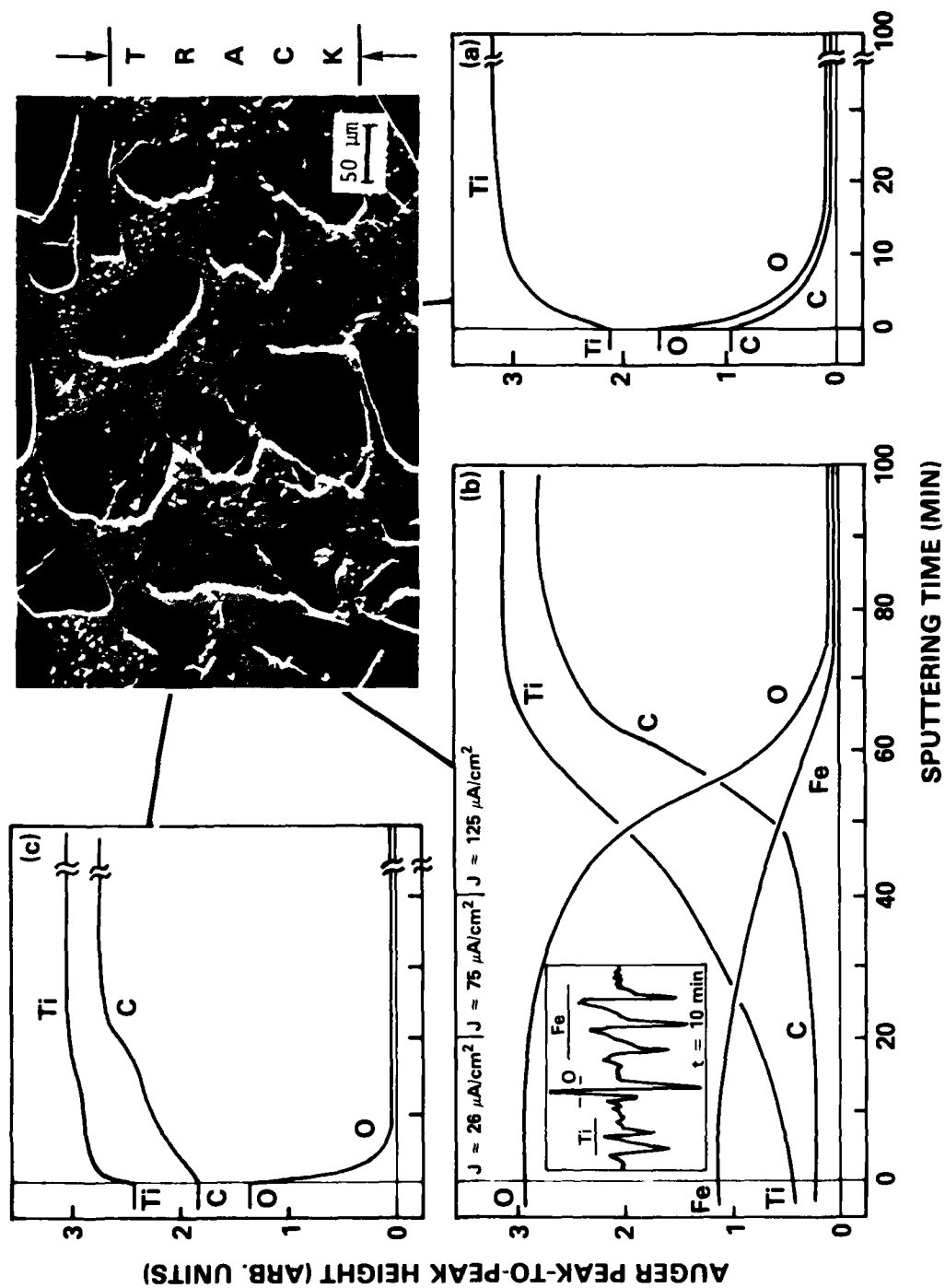
Fig. 6 – Auger sputter depth profiles of a portion of the 20 pass wear track on the Ti implanted TiC/Ti disk, 80-5. Three features of the track shown in the circles in the SEM photo, were profiled concurrently during ion milling: a) non-worn Ti alloy matrix (away from the visible dendritic phase); b) a debris flake attached to a TiC particle; and c) a debris-free carbide surface.

lower wear rate than do WC cutting tools (10). Although the contacts were, of course, at a much lower temperature during these tests, it is speculated that adhesive welding may have occurred as a result of the solution wear of WC in steel.

The difference in friction and wear between the TiC/Ti and WC/Ti samples may also be partially explained by the relative hardnesses of the TiC and WC particles (2600 kg/mm and 1500 kg/mm, respectively, Ref. 2), since, in general, harder materials exhibit superior friction and wear resistance. Also, a considerably lower degree of matrix hardening (28% maximum, Ref. 2) was achieved for the WC injected disks as a result of partial carbide dissolution during processing than for the TiC/Ti disk (122% maximum hardening, Ref. 2). Consequently, both the carbides and matrix of the WC/Ti disks were softer and more susceptible to wear than those of the TiC/Ti disk. The Al matrix of the TiC/Al disks was much softer than the Ti matrix samples (2), and did not harden appreciably as a result of laser processing (2). However the presence of the TiC particles allowed for lower friction and wear than for the WC/Ti disks.

The injected carbide particles provided the excellent wear resistance observed for the nonimplanted disks. The large carbide sizes and high carbide volume % of the disks insured that many, if not the majority, of contact events between ball and disk took place at the carbides. This explains, then, the lack of surface scratching, grooving or deformation on these samples during most of the tests made before implantation. On the low % carbide WC/Ti disk, 80-20, however, the matrix phase was more accessible to the ball, allowing for more debris accumulation on the ball to occur by the process of "prow formation", described by Antler and others (11-13). This process initiates by the adhesive transfer of material from the contact member with the larger surface area to the smaller contact, (e.g. from a disk to a ball). The transferred debris may then cause secondary wear by abrasion (12).

Apparently, in the case of tracks on disk 80-20, debris accumulated on the ball was able to produce abrasive damage and roughening on the matrix phase surface. After repeated passes over the test tracks, the debris was backtransferred to the disk so that, it is speculated, the onset of severe stickslip friction (at approximately the 10th pass) during testing corresponded to debris material on the ball making contact with debris smeared on the carbides, with resultant increases in area of contact and adhesive welding. The debris on the carbides appear to consist of stacked overlapping layers of material, a typical fea-

ture of wear debris produced by prow formation (11). The occurrence of stickslip and debris formation during test #2 on TiC/Al sample 80-31 (Table II) is further evidence that inhomogeneities in carbide concentration are the weakest link in the wear resistance of these carbide/metal composites, with the carbide poor regions providing the initiation points for adhesive wear.

Ti implantation of the LMPI disks promoted debris formation and increased friction during dry sliding as a result, it is suggested, of 1) softening of the carbide particles (discussed further below) and 2) enhanced reactivity of the disk surfaces due to the presence of excess Ti on both matrix and carbide phases. In contrast to the nonimplanted disks, the adhesive interactions between the balls and the disks were strong enough to produce high friction coefficients, occasional stickslip, and even some material transfer to the carbides, during the first passes on the implanted surfaces. The large amounts of debris generated on the implanted disks, and their chemical analyses, were further indications of an increased reactivity/affinity between the steel and the Ti implanted surfaces.

The extreme chemical activity of titanium insures strong adhesion between titanium alloys and contacting surfaces. Indeed it is the resulting high adhesive friction and galling wear during sliding contact which prohibits the use of these alloys in applications requiring wear resistance. Buckley attributes this high surface reactivity to the low d-band characteristic of the metallic bonding of titanium (14). That is, since relatively little d-band electron energy is involved in the bulk metallic bonding, very strong d-band interactions can take place between titanium atoms and contacting metal and insulator surfaces.

High fluence ion implantation has been found to cause softening in many ceramic and cermet materials (15,16). In particular, WC was found to soften after Ti implantation to a fluence of 5×10^{17} Ti/cm^2 at 400 keV (16). Ti implantation seems to have softened the carbides of the LMPI samples, as evidenced by the scratches on the carbides of the TiC/Ti disk after implantation (Fig. 5), and by the carbide debris found in several of the post-implantation tracks on other disks.

Apparently, the softer implanted layers wore off, contributing to the accumulation of debris on the ball surfaces during the initial passes of testing. Thus, decreased hardness of the carbide phase, and the increased adhesion, promoted sufficient debris accumulation on the ball to produce visible wear of the Ti and Al alloys. The large amounts of debris backtransferred to

the disks (selectively to the carbides) is believed to have produced the severe stickslip friction during the latter parts of the tests. The high coeffs. of friction of the implanted disks, then, reflect the increased forces required to shear the transfer film contacts at the ball/debris/disk interface.

The friction and wear properties of the TiC/Ti disk were degraded less severely than those of the other disks. The matrix phase appeared undamaged after testing, perhaps due to immediate adhesion and backtransfer of debris on the ball to the carbides. Analysis of debris on the TiC/Ti tracks and on the corresponding ball surfaces could not definitively determine the origen of the debris, since both matrix and carbide phases of the disk (as well as the implant species) consisted of Ti. However, the undamaged appearance of the matrix phase, as well as the presence of Ti on ball surfaces run against the nonimplanted TiC/Al disks, indicate that debris material was sheared initially from the implanted TiC particles.

Although there was considerable debris on the disk (Fig. 5), stickslip disappeared after the first few passes. Oxidation of the steel and disk debris after backtransfer to the disk (as indicated by the Auger data, Fig. 6), may have contributed to the prevention of the severe stickslip characteristic by diminishing the chemical reactivity at the contact interface.

CONCLUSION

1. High galling wear resistance during dry sliding against steel is provided by high carbide volume % LMPI carbide/metal composites. However, since carbide-poor regions serve as nucleation sites for adhesive wear, local inhomogeneities in carbide density are an important factor in the determination of galling wear resistance.

2. The lowest friction and wear behavior was exhibited by the TiC/Ti sample. This can be attributed to the superior hardness of this disk, and to the lower degree of compatibility (i.e. mutual solid solubility) of TiC/steel couples, as compared to WC/steel couples.

3. Stickslip friction, the result of adhesive microwelding at the contact interface, can occur when the reactivity of the materials is very great, as was the case on the first pass on the TiC/Ti disk following implantation . Severe stickslip, leading to high frictional losses, however, is most frequently indicative of a large amount of debris coverage on both counterfaces with resulting debris-debris contact and concommitant increases in contact area, adhesion and backtransfer.

4. High fluence Ti-implantation pro-

duced increased friction and wear of the LMPI disks as a result of the a) enhanced reactivity of the surfaces provided by the excess Ti and b) softening of the carbides.

REFERENCES

1. Ayers, J. D., R. J. Schaefer and W. P. Robey, J. Met. 33(8), 19-23 (1981).

2. Ayers, J. D., and R. N. Bolster, Wear 93, 193-205 (1984).

3. Singer, I. L., and R. A. Jeffries, J. Vac. Sci. Technol. A1, 317 (1983).

4. Singer, I. L. and R. A. Jeffries, "Friction, Wear and Deformation of Soft Steels Implanted with Ti or N" in Mat. Res. Soc. Symp. Proc. vol 27, p. 667, Elsevier, N. Y. (1984).

5. Singer, I. L., "Tribomechanical Properties of Ion Implanted Metals" in Mat. Res. Soc. Symp. Proc. vol 27, p 585, Elsevier, N. Y. (1984).

6. Dillich, S. A., R. N. Bolster and I. L. Singer, "Friction and Wear Behavior of a Cobalt - Based Alloy Implanted with Ti or N" in Mat. Res. Soc. Symp. Proc. vol 27, p 637, Elsevier, N. Y. (1984).

7. Singer, I. L., and T. M. Barlak, Appl. Phys. Lett. 43, 457-459 (1983).

8. E. Rabinowicz, "Friction and Wear of Materials", 75, John Wiley and Sons Inc., N. Y. (1966).

9. Rabinowicz, E., ASLE Trans. 14, 198-205 (1971).

10. Kramer, B. M., ASME J. of Eng. Ind. 102, 303-309 (1980).

11. Antler, M. "Sliding Wear of Metallic Contacts" in Electrical Contacts 80, p 3, Illinois Institute of Technology, (1980).

12. Antler, M., ASLE Trans. 13, 2152-2161 (1962).

13. Cocks, M., J. of Appl. Phys. 33, 2152-2161 (1962).

14. Buckley, D. H., "Surface Effects of Adhesion, Friction, Wear and Lubrication" Tribology Series 5, 388-394, Elsevier, N. Y. (1981).

15. Dearnaley, G., B. James, D. J. Mazey and F. J. Minter, "The Micro Hardness of Nitrogen Ion Implanted Cobalt Cemented Tungsten Carbide", Proc. Plansee Conf., Reute, Austria (1985).

16. Burnett, P. J. and T. F. Page," The Effects of Ion Implantation on the Surface Mechanical Properties of some Engineering Hard Materials," in Science of Hard Materials II, Conf. Proc, Rhodes, Greece, 1984, in print.

END

DTIC

6 — 86